PHILOSOPHICAL TRANSACTIONS A

royalsocietypublishing.org/rsta

CC BY

Research

Cite this article: Sommariva R *et al.* 2026 Tropospheric Ozone Assessment Report II: Ozone distribution and variability in the oceanic and polar regions. *Phil. Trans. R. Soc. A* **384**: 20250269.
https://doi.org/10.1098/rsta.2025.0269

Received: 31 December 2025
Accepted: 16 June 2026

One contribution of 8 to a theme issue 'Tropospheric Ozone Assessment Report II'.

Subject Areas:
environmental chemistry, atmospheric science, atmospheric chemistry

Keywords:
tropospheric ozone, atmospheric composition, ozone trends, linear mixed-effects modelling, marine troposphere, polar troposphere, oceans, Arctic, Antarctic

Authors for correspondence:
Alfonso Saiz-Lopez
e-mail: a.saiz@csic.es
Roberto Sommariva
e-mail: rs445@le.ac.uk

†These authors contributed equally to the work.

Supplementary material is available online at https://doi.org/10.6084/m9.figshare.c.8638418.

THE ROYAL SOCIETY PUBLISHING

Tropospheric Ozone Assessment Report II: Ozone distribution and variability in the oceanic and polar regions

Roberto Sommariva[1,2,†], Theodore K. Koenig[3,†], Takashi Sekiya[4], Alba Badia[5], Yugo Kanaya[4], Andrea Mazzeo[6], Marios Panagi[7], Katie A. Read[8], Matthew J. Rowlinson[8], Maria R. Russo[9,10], Nathan Luke Abraham[9,10], Jose A. Adame[11], Kai-Lan Chang[12,13], Jesper H. Christensen[14], Wanmin Gong[15], Fernando Iglesias-Suarez[16], Ulas Im[14,17], Patrick Jöckel[18], Debra E. Kollonige[19], Mariano Mertens[18,20], Raeesa Moolla[21], Ryan M. Stauffer[19], Anne M. Thompson[19,22], Kenjiro Toyota[15] and Alfonso Saiz-Lopez[23]

[1]School of Geography, Earth and Environmental Sciences, University of Birmingham, Birmingham, UK
[2]School of Chemistry, University of Leicester, Leicester, UK
[3]Division of Environment and Sustainability, The Hong Kong University of Science and Technology, Hong Kong, China
[4]Japan Agency for Marine-Earth Science and Technology (JAMSTEC), Yokohama, Kanagawa, Japan
[5]Barcelona Supercomputing Center, Barcelona, Spain
[6]Lancaster Environment Centre, Lancaster University, UK
[7]Climate and Atmosphere Research Center, The Cyprus Institute, Nicosia, Cyprus
[8]National Centre for Atmospheric Science (NCAS), WACL, Department of Chemistry, University of York, York, UK
[9]National Centre for Atmospheric Science (NCAS), Cambridge, UK
[10]Yusuf Hamied Department of Chemistry, University of Cambridge, Cambridge, UK
[11]Atmospheric Sounding Station, El Arenosillo Observatory, Instituto Nacional de Técnica Aeroespacial (INTA), Mazagón-Huelva, Spain

© 2026 The Authors. Published by the Royal Society under the terms of the Creative Commons Attribution License http://creativecommons.org/licenses/by/4.0/, which permits unrestricted use, provided the original author and source are credited.

Downloaded from royalsocietypublishing.org/rsta/article-pdf/doi/10.1098/rsta.2025.0269/6174177/rsta.2025.0269.pdf
by German Aerospace Centre (DLR) user
on 27 October 2026

[12]Cooperative Institute for Research in Environmental Sciences (CIRES), University of Colorado – Boulder, Boulder, Colorado, USA
[13]NOAA Chemical Sciences Laboratory, Boulder, Colorado, USA
[14]Aarhus University, Department of Environmental Science, Roskilde, Denmark
[15]Environment and Climate Change Canada, Toronto, Canada
[16]Predictia Intelligent Data Solutions S.L., Santander, Spain
[17]Ecole Polytechnique Fédérale de Lausanne (EPFL), Lausanne, Switzerland, Lausanne, Switzerland
[18]Deutsches Zentrum für Luft- und Raumfahrt, Institut für Physik der Atmosphäre, Oberpfaffenhofen, Germany
[19]Earth Sciences Division, NASA Goddard Space Flight Center, Greenbelt, Maryland, USA
[20]Faculty of Aerospace Engineering, Section Operations and Environment, Delft University of Technology, Delft, The Netherlands
[21]School of Geography, Archaeology and Environmental Studies, University of the Witwatersrand, Johannesburg, South Africa
[22]University of Maryland – Baltimore County, Baltimore, Maryland, USA
[23]Department of Atmospheric Chemistry and Climate, Institute of Physical Chemistry Blas Cabrera (CSIC), Madrid, Spain

RS, 0000-0002-2728-5814; TKK, 0000-0002-3756-4315; TS, 0000-0002-2319-7753; AB, 0000-0003-0906-8258; YK, 0000-0001-9354-3116; AM, 0000-0002-7109-0934; MP, 0000-0003-0422-2922; KAR, 0000-0002-4044-455X; MRR, 0000-0003-1061-7007; NLA, 0000-0003-3750-3544; JAA, 0000-0002-6302-7193; K-LC, 0000-0001-5812-3183; JHC, 0000-0002-6741-5839; WG, 0000-0003-3635-0857; FI-S, 0000-0003-3403-8245; UI, 0000-0001-5177-5306; PJ, 0000-0002-8964-1394; DEK, 0000-0002-6597-328X; MM, 0000-0003-3549-6889; RM, 0000-0001-8049-1660; RMS, 0000-0002-8583-7795; AMT, 0000-0002-7829-0920; KT, 0000-0001-9280-5305; AS-L, 0000-0002-0060-1581

Oceanic and polar regions are critical for global atmospheric processes, but an evaluation of ozone distributions and trends in these regions has been missing. In this assessment, part of the TOAR-II project, we report lower atmosphere ozone concentrations over open oceans and polar regions: with data from ships, buoys, aircraft and ground sites from 1975 to 2023, this is the most comprehensive dataset yet. Ozone trends were determined using Linear Mixed-effects Modelling (LMM). In most regions, trends have been modest since the mid-1970s (<1 nmol mol^{-1} per decade), positive in the mid-latitudes and tropical regions (with medium-low certainty), negative in the North and Tropical Pacific (with low and high certainty, respectively), increasing in Antarctica and decreasing in the Arctic. Seasonal effects often influence the long-term trends in extra-tropical regions. Five global and one hemispheric models were used to aid the interpretation of the sparse observations. The seasonal cycles are reasonably well reproduced, although models disagree with each other and with the observations on the distribution of ozone, especially in the tropics and in the Arctic. Changes in methane, iodine, shipping emissions, nitrogen oxides emissions, and terrestrial and marine volatile organic compound are likely to be important drivers for ozone over the oceans, although specific attributions are uncertain owing to insufficient data.

This article is part of the theme issue 'Tropospheric Ozone Assessment Report II'.

1. Introduction

Tropospheric ozone (O_3) is a short-lived atmospheric pollutant and climate forcer, contributing an estimated 0.47 W m^{-2} to the effective radiative forcing [1]. The tropospheric ozone burden is

Downloaded from royalsocietypublishing.org/rsta/article-pdf/doi/10.1098/rsta.2025.0269/6174177/rsta.2025.0269.pdf
by German Aerospace Centre (DLR) user
on 27 October 2026

determined by the emission of precursors—nitrogen oxides (NO_x), carbon monoxide (CO), volatile organic compounds (VOCs) and methane (CH_4)—together with chemical losses, atmospheric transport, surface deposition and stratosphere-troposphere exchange (STE) [2–4]. The IPCC AR6 [5] estimated that the global tropospheric ozone burden has increased by approximately 40% from 1850 to the early twenty-first century, a trend that is confirmed by estimates from the available observations and model studies [4,6–8], although observations are biased towards the Northern Hemisphere. Long-term ozone records highlight hemispheric contrasts and atmospheric transport influences, and underscore the scarcity of available observations [9].

The oceans and the polar regions cover over 70% of the Earth's surface; it is essential to understand ozone changes in these environments because of their role in intercontinental pollution transport, their implications for climate and their impacts on air quality in coastal areas—where much of the world population lives and which can be strongly affected by marine air masses [10]. According to historical ship-borne measurements, ozone trends over the oceans differ from those over the continents [11] as oceanic and polar ozone is shaped by processes distinct from those over the continents, particularly long-range transport and local emissions of precursors, such as CH_4 and shipping NO_x (NO, NO_2). Net chemical loss of ozone is a key feature over the remote oceans, driven by HO_x (OH, HO_2), bromine (Br) and iodine (I) radicals [12,13]. The Arctic and the Antarctic are characterized by sources of reactive gases from the snowpack: halogens, in particular, can rapidly destroy ozone during the boreal spring [14], while NO_x formed via photolysis of nitrate preserved in the surface snowpack can perturb ozone levels in the pristine atmosphere, such as over the Antarctic plateau and its downwind areas [15–17]. Dry deposition of ozone is considered to be important on oceanic surfaces [18,19], but generally slow on sea ice and polar ice caps; yet, it is not negligible for the variability of surface ozone at high latitudes [20,21].

The Tropospheric Ozone Assessment Report (TOAR, http://igacproject.org/activities/TOAR) is an International Global Atmospheric Chemistry-sponsored activity that aims to provide the scientific community with up-to-date scientific assessments of tropospheric ozone [22]. TOAR-I focused on ozone distribution and trends from the perspective of climate [8], health [23] and ecosystems [24], but a complete assessment of our understanding of ozone over the open oceans and the polar regions has been missing. Despite their importance, these regions remain much less studied than the continents. In part, this is owing to practical issues: taking measurements—especially long-term measurements—in remote environments is logistically and technically challenging, leading to sparse and geographically uneven observations.

In this assessment, we aim to fill this knowledge gap using the most comprehensive dataset of observations of ozone from ships, buoys, aircraft and ozonesondes assembled to date [25], to complement the TOAR-II database and gain a better insight on the geographical distribution, temporal variability (seasonality, interannual and long-term trends) and net chemical tendencies of ozone over oceanic and polar regions.

2. Ozone observations and modelling

(a) Observational data coverage

The dataset used in this assessment consists of ozone observations from mobile platforms—ships, buoys, aircraft and ozonesondes—and from selected ground-based observatories in coastal areas, the Arctic and the Antarctic. The ground sites, chosen for their geographical location and representativeness of oceanic and polar regions, were taken from the TOAR-II database [Worden *et al.*, this issue]. This is the largest dataset of oceanic and polar ozone observations from mobile platforms ever compiled and consists of over 600 000 individual data points, covering the period 1975–2023 (supplementary material, tables S1 and S2). For a detailed description of the dataset, how it was assembled and processed, see [25]; additional information specifically related to ozonesondes can be found in [26].

Downloaded from royalsocietypublishing.org/rsta/article-pdf/doi/10.1098/rsta.2025.0269/6174177/rsta.2025.0269.pdf
by German Aerospace Centre (DLR) user
on 27 October 2026

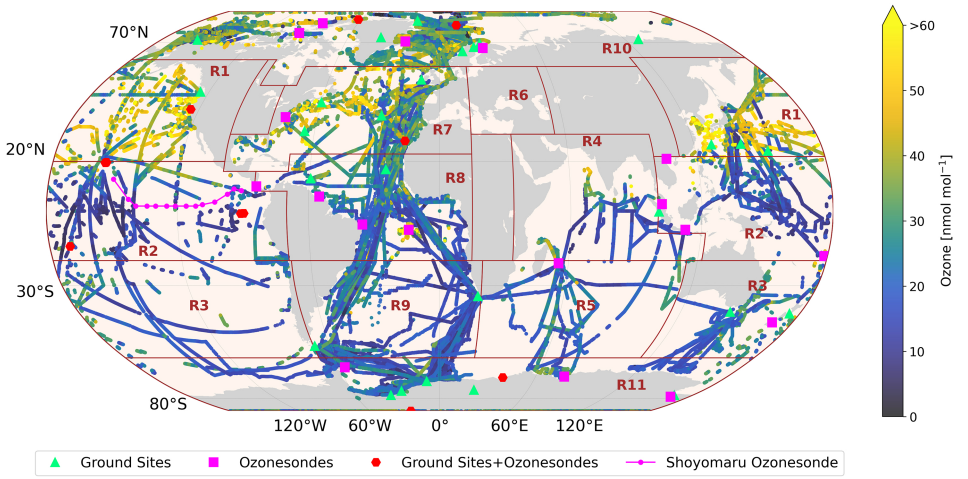


Figure 1. Ozone measurements from mobile platforms in the oceanic and polar regions between 1975 and 2023. Also shown are the locations of the ozonesondes launch sites, including the track of the Shoyomaru ozonesonde launchpad, and selected ground observatories (coastal and polar) from the TOAR-II database. The upper limit of the colour bar is capped at 60 nmol mol^{-1}: all values exceeding the cap are displayed in the same colour.

For this assessment, the ozone data were filtered by two additional criteria: (i) minimal continental contact in the last 72 hours, as determined using chemical tracers and trajectories [25] and (ii) altitude below 2 km above sea level—except for the polar ground sites known to be inside the boundary layer, which were included regardless of altitude. The resulting dataset was divided into nine open ocean and two polar regions (figure 1; supplementary material, table S3). Region R6, which covers the Eastern Mediterranean, Black and Caspian Seas, was excluded from the analysis because it is too heavily influenced by the surrounding land masses.

Data coverage in the oceanic and polar regions is typically sporadic because, with the exception of the few ground observatories and ozonesonde launch sites, most of the data in these regions come from field campaigns on mobile platforms, which are limited in both time and space. Moreover, many regions have limited or no data prior to the 1990s ([25]; see also supplementary material, figures S5–S7). Generally, there are more data in the Northern Hemisphere (R1, R7), followed by the tropical Atlantic and Pacific (R2, R8); in the Southern Hemisphere, only the South Atlantic region (R9) is extensively sampled (supplementary material, table S2). Other TOAR-II studies (e.g. [27,28]) have noted there are more observations from the North and tropical Atlantic, while the tropical Pacific and the Southern Hemisphere oceans are undersampled. Limited and uneven data coverage poses a fundamental challenge in identifying patterns and trends in the distribution of ozone over the open oceans and polar regions.

(b) Models

Global chemistry-climate and chemistry-transport models are useful to supplement sparse observations and investigate the ozone variability across the undersampled oceanic and polar regions. Five global models were used in this assessment: CHASER [13], CAM-Chem [29,30], UKESM [31,32], EMAC [33], GISS-E2.1 [34,35]. In addition one hemispheric model—DEHM [36,37]—was used. Each model simulates tropospheric ozone using different treatments of chemistry, emissions and transport. In particular, halogens (Cl, Br and I), which are increasingly recognized as key controls on ozone over remote marine regions [38,39], are treated differently in each model. For instance, full halogen chemistry is included only in CHASER and CAM-Chem, while DEHM only includes a blowing-snow Br source. Details on the global models used in this assessment can be found in the supplementary material.

Downloaded from royalsocietypublishing.org/rsta/article-pdf/doi/10.1098/rsta.2025.0269/6174177/rsta.2025.0269.pdf
by German Aerospace Centre (DLR) user
on 27 October 2026

3. Geographical distribution and seasonality

Ground-level observations from ships, buoys, coastal and polar observatories compared to the multi-model mean (MMM) of seasonal surface ozone distributions are shown in figure 2; the measured and modelled mean annual cycles for each region are shown in figure S1 in the supplementary material, and the mean latitudinal transects in figure S2 in the supplementary material. Despite sparse observations, the MMM broadly captures the latitudinal and seasonal distribution of surface ozone reasonably well, with a strong gradient between the Northern and Southern Hemispheres (figure 2). In some regions, such as the Indian Ocean where no observations are available between March and September, the seasonal cycle is incomplete; Elshorbany *et al.* [40] also highlighted that the absence of consistent measurements in the Indian Ocean limits our ability to assess ozone trends in this region with confidence. There are considerable differences between the six models, as shown by the large spread in their results (figure 2, bottom). In tropical regions and during springtime, models disagree more (up to 60%), possibly owing to different positions of the intertropical convergence zone (ITCZ) and the chemical equator [41] related to the difficulty for models to adequately capture atmospheric dynamics. Large differences between the models are also found in the Arctic during the Northern winter (December–January–February, DJF), when uncertainties in the model representations of dry deposition, vertical mixing or halogen chemistry contribute to the large model spread [20,42].

Seasonal variations in tropospheric ozone are most pronounced at mid-latitudes. In the Northern Hemisphere, ozone over the Pacific and Atlantic oceans shows clear cycles with pronounced spring maxima (March–April–May, MAM) and summer minima (June–July–August, JJA). The spring maximum reflects enhanced transport of continental air masses by active mid-latitude storms, combined with a longer chemical lifetime under cooler and moderately sunny conditions. Conversely, the summer minimum arises from faster ozone destruction owing to higher temperatures and more intense sunlight, as well as the influence of subtropical high-pressure systems limiting long-range transport. In the Southern Hemisphere, both the Pacific and Atlantic oceans display similar cycles, with the highest concentrations in August (Southern winter)—reflecting slower ozone destruction under cooler, less sunny conditions—and the lowest in December–January (Southern summer). The MMM can reproduce these seasonal patterns, though with a slight delay in the spring maximum and weaker amplitude. All models show a positive bias in the Northern Hemisphere (0–5 nmol mol^{-1}) and a negative bias in the Southern Hemisphere (6–9 nmol mol^{-1}). Under-represented sources of NO_x via nitrate photolysis from aerosols [43,44] and polar ice caps [17] potentially play a role, especially over Southern oceans where conditions are consistently NO_x-limited.

In the tropics, ozone concentrations are lower than in the mid-latitudes (supplementary material, figure S2), and the seasonal variability is weaker. Elevated ozone from the winter hemisphere extends seasonally, and the ozone minimum shifts either side of the equator. The models generally fail to reproduce the seasonal patterns in tropical regions, especially during winter in the tropical Pacific and during summer in the tropical Atlantic (figure 2). There is not a consistent annual cycle in ozone across tropical regions or at most individual sites, but a quasi-annual cycle is apparent in the regional averages and at most individual sites (supplementary material, figure S1). It is likely that this effect is owing, at least in part, to interannual variability in the position of the chemical equator [41].

In the polar regions, the seasonal patterns are very different between hemispheres. Neither the MMM nor the individual models (supplementary material, figure S2) reproduce the observed polar seasonal cycles. In particular, the Arctic spring minimum is not captured by any of the models: the discrepancy can be linked to ozone depletion events (ODEs), which are frequent in the Arctic during springtime and drive the near-surface ozone minimum in contrast to the springtime maximum at lower latitudes [45–47]. ODEs arise primarily from catalytic destruction of ozone by reactive Br released from snowpack [48,49] and blowing snow [50,51] over sea ice, initiated by photochemical reactions within/on snow particles and propagated through heterogeneous reactions

Downloaded from royalsocietypublishing.org/rsta/article-pdf/doi/10.1098/rsta.2025.0269/6174177/rsta.2025.0269.pdf
by German Aerospace Centre (DLR) user
on 27 October 2026

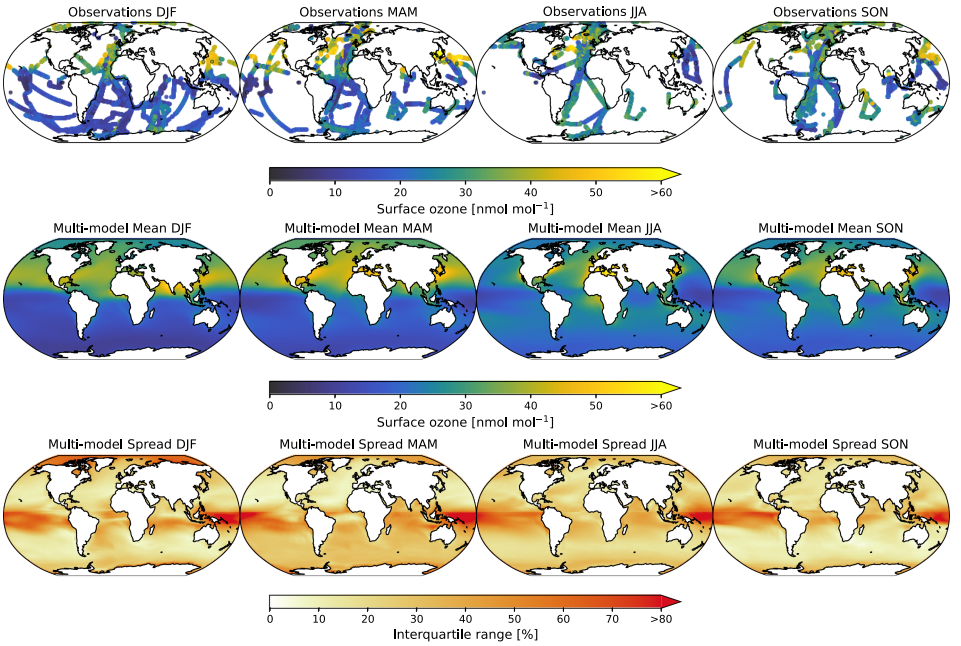


Figure 2. Seasonal surface ozone in oceanic and polar regions: measured mean concentrations from ships, buoys and ground sites (top), MMM (middle) and multi-model spread (interquartile range, bottom). The upper limits of the colour bar are capped at 60 nmol mol^{-1} and 80% spread: all values exceeding the caps are displayed in the same colour. The seasonal cycles and latitudinal transects, measured and calculated by each model, are shown in the supplementary material (figures S2 and S3).

on aerosol surfaces [52–55]. Recent studies [46,47] have demonstrated that models need to incorporate a process representation of halogen emissions from the snowpack to be able to reproduce the observed spring ozone minimum in the Arctic (supplementary material, figure S3).

4. Ozone trends

(a) Calculation of ozone trends

The data used in this assessment have been collected from multiple platforms, instruments and locations over five decades [25]. Therefore, the calculation of regional ozone trends has to explicitly account for the unavoidable discrepancies between different records—e.g. resulting from instrumental sensitivity and/or spatio-temporal discontinuity. For this reason, the methodology used in the other TOAR-II assessments and described in [56] is not applicable here; instead, we used a Linear Mixed-effects Modelling (LMM) approach, which takes into account potential offsets and trend variability between different records [57,58]. The LMM method and trend calculation are described in detail in the supplementary material, and the results are shown in table 1 and figures 3 and 4. In the following discussion, we refer to the TOAR-II statistical guidelines [56], which use the *p*-value of the LMM fit as a metric of its reliability—consistent with the treatment of uncertainties in the IPCC reports [59]: very high certainty (≤0.01), high certainty (0.01–0.05), medium certainty (0.05–0.1), low certainty (0.1–0.33) and very low certainty or no evidence (≥0.33).

We calculated the trends using monthly ozone means (figure 4) and included site-specific and seasonal terms (figure 3; supplementary material, figure S10); since the LMM methodology works best when all data sources have a sufficient number of points, we included only records with at least 60 months of data coverage—after the chemical tracers, trajectory and altitude filters were applied, as described above. As noted by Cooper *et al.* [60], the rate of change of ozone is not necessarily constant within the whole trend period; therefore, we also calculated the trends

Downloaded from royalsocietypublishing.org/rsta/article-pdf/doi/10.1098/rsta.2025.0269/6174177/rsta.2025.0269.pdf
by German Aerospace Centre (DLR) user
on 27 October 2026

Table 1. Ozone trends (nmol mol^{-1} per decade), uncertainties (2-σ) and p-values calculated with the LMM method using data filtered ('60mo') and not filtered ('All') by the 60-month criterion. The trends are calculated from the start of each dataset and from 1990, 1995 and 2000. The blue and red backgrounds indicate positive and negative trends, respectively, while the shading indicates the level of certainty (very high, high, medium and low).

Region	Data	start-2023		1990-2023		1995-2023		2000-2023	
		Trend ± 2-σ	p	Trend ± 2-σ	p	Trend ± 2-σ	p	Trend ± 2-σ	p
North Pacific	60mo	–	–	−1.07 ± 1.48	0.15	−1.05 ± 1.49	0.16	−1.01 ± 1.53	0.19
(R1)	All	−0.64 ± 1.10	0.24	−0.41 ± 1.07	0.45	−0.47 ± 1.08	0.38	−0.48 ± 1.12	0.39
Tropical Pacific	60mo	−0.09 ± 0.34	0.59	−0.08 ± 0.50	0.76	−0.06 ± 0.63	0.85	−0.56 ± 0.50	0.03
(R2)	All	−0.15 ± 0.98	0.75	−0.04 ± 1.02	0.94	−0.01 ± 1.06	0.99	−0.58 ± 1.11	0.30
South Pacific	60mo	+0.13 ± 0.32	0.42	+0.53 ± 0.61	0.08	+0.41 ± 0.22	<0.01	+0.27 ± 0.33	0.10
(R3)	All	+0.23 ± 0.23	0.04	+0.46 ± 0.32	<0.01	+0.45 ± 0.23	<0.01	+0.30 ± 0.32	0.06
South Indian	60mo	–	–	+2.06 ± 0.72	<0.01	+2.06 ± 0.72	<0.01	+1.88 ± 0.83	<0.01
(R5)	All	–	–	+1.68 ± 0.68	<0.01	+1.69 ± 0.68	<0.01	+1.54 ± 0.79	<0.01
North Atlantic	60mo	+0.19 ± 0.82	0.64	+0.17 ± 0.84	0.68	−0.41 ± 1.21	0.49	−0.67 ± 1.28	0.29
(R7)	All	+0.75 ± 0.79	0.06	+0.64 ± 0.83	0.12	−0.43 ± 0.88	0.32	−0.65 ± 0.97	0.18
Tropical Atlantic	60mo	+0.51 ± 0.68	0.14	+0.50 ± 0.80	0.21	+0.59 ± 0.81	0.15	+0.63 ± 0.89	0.15
(R8)	All	+1.01 ± 0.77	0.01	+0.85 ± 0.85	0.04	+0.68 ± 0.97	0.16	+0.68 ± 1.03	0.19
South Atlantic	60mo	–	–	+0.09 ± 0.43	0.67	+0.05 ± 0.43	0.83	+0.32 ± 0.47	0.17
(R9)	All	+1.35 ± 0.94	<0.01	+0.08 ± 0.51	0.76	−0.37 ± 0.43	0.09	+0.20 ± 0.59	0.50
Arctic	60mo	+0.05 ± 0.37	0.77	+0.06 ± 0.40	0.75	−0.29 ± 0.43	0.18	−0.58 ± 0.54	0.03
(R10)	All	+0.06 ± 0.36	0.73	+0.00 ± 0.35	0.99	−0.41 ± 0.38	0.03	−0.74 ± 0.46	<0.01
Antarctic	60mo	+0.43 ± 0.11	<0.01	+0.58 ± 0.29	<0.01	+0.47 ± 0.30	<0.01	+0.24 ± 0.27	0.08
(R11)	All	+0.64 ± 0.52	0.01	+0.55 ± 0.33	<0.01	+0.36 ± 0.34	0.03	+0.19 ± 0.32	0.25

level of certainty: very low, low, medium, high, very high

starting from 1990, 1995 and 2000 to understand when they may have changed in magnitude or certainty (table 1; supplementary material, figure S4). The differences in calculated trends with different starting years can be large and in some instances (e.g. Antarctic) exceed 2-σ, reflecting the fact that the underlying change in ozone is highly variable and dynamic. The deseasonalized and site-corrected averages (figure 4; supplementary material, figures S4 and S5) give some indication of the underlying trend, as discussed further below.

The 60-month criterion is deemed sufficient for the reliability of the seasonal means of a given record, and hence determines more accurately the potential site offsets [58]; however, it excludes some data—at most approximately 25% and typically <10% of the total dataset—mostly from mobile platforms (supplementary material, table S2). The ozone trends in figure 4 are therefore weighted towards observations from ozonesondes and ground sites (supplementary material, table S1). Ozone trends calculated without the 60-month criterion (supplementary material, figure S3) are generally greater in magnitude—more than 1-σ difference but less than 2-σ (table 1)—and in certainty, although they agree in some regions such as the Antarctic and the tropical Atlantic. We attribute this effect to potential representativeness and specification biases, possibly leading to false attribution of divergent trends to site-specific effects (see below). Nonetheless, the additional sources greatly extend spatial coverage within regions, and we cannot exclude the possibility that these trends are more representative.

We conducted bootstrap runs of the LMM analysis to calculate the trends at the individual measurement sites selected via the 60-month criterion (supplementary material, table S1), assess the site-specific effects and determine how representative they are of their respective regions (supplementary material, table S4) . Offsets between sites are as large as 29 ± 6 nmol mol^{-1} (Arctic, figure 3), and between seasonal cycles up to 22 nmol mol^{-1} peak-to-peak (North Pacific; supplementary material, figure S9), much greater than the fitted trends 1.07 ± 0.74 nmol mol^{-1} per decade. The LMM therefore consistently accounts for the offset between sites, but in regions like the tropics, where intra-annual variability is not well captured by a consistent seasonal cycle, it has limitations. The fitted peak-to-peak seasonal cycle (3.6 and 2.5 nmol mol^{-1} in the tropical Pacific and Atlantic, respectively) is less than the mean seasonal peak-to-peak difference (5.3 and 4.9 nmol mol^{-1}, respectively); inspection of the data reveals a quasi-annual range >10 nmol mol^{-1} appearing inconsistently across calendar months (figure 4). In these regions and in the South Pacific, the trends fitted by the LMM for individual sites are much smaller than the corresponding regional trend, limited by insufficient constraint on intra-annual variability (figure 3). In regions where the seasonal cycles are consistent and well fitted (e.g. North Pacific; supplementary material, figure

Downloaded from royalsocietypublishing.org/rsta/article-pdf/doi/10.1098/rsta.2025.0269/6174177/rsta.2025.0269.pdf
by German Aerospace Centre (DLR) user
on 27 October 2026

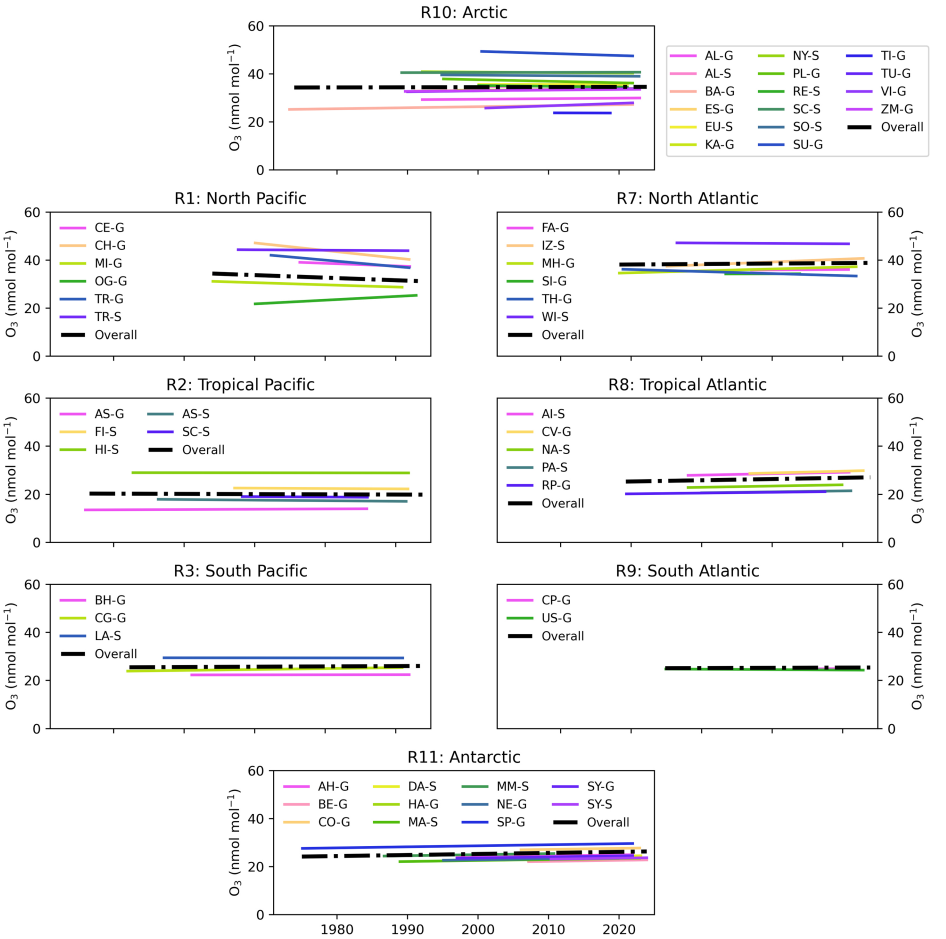


Figure 3. Near-surface ozone trends calculated at individual sites with the LMM method. Data are filtered by the 60-month criterion, and trends are calculated from the beginning of the dataset at each site. The site codes are listed in the supplementary material (table S3).

S9) and numerous sites with extended coverage are available, the LMM fits site-specific trends in addition to offsets.

The limited ability to fit site-specific trends manifests as a covariance between the trends fitted for sites within a region, while the covariance between site-specific trends and the regional trend is weak. Subtracting the difference between the site-specific trend line and the regional trend line (figure 3) and the seasonal cycle (supplementary material, figure S10) from each monthly mean gives the 'corrected' mean shown in figure 4, which roughly corresponds to the data the trend is fitted to, after removing larger sources of variance, and is mathematically equivalent to the monthly LMM residual about the regional trend line. This procedure gives some indication of underlying nonlinear trends in the data—e.g. a shift in the North Atlantic in the late 1990s—although the possibility remains of individual sites creating apparent trends, such as Barrow in the Arctic (see below).

(b) Regional ozone trends

(i) Polar regions

The Antarctic shows increasing ozone levels by $+0.43 \pm 0.11$ nmol mol^{-1} per decade between 1975 and 2023 with very high certainty ($p < 0.01$). Figure 4 shows decreasing ozone levels in the 1980s,

Downloaded from royalsocietypublishing.org/rsta/article-pdf/doi/10.1098/rsta.2025.0269/6174177/rsta.2025.0269.pdf
by German Aerospace Centre (DLR) user
on 27 October 2026

followed by a trend reversal in the early 1990s. While the earliest data are from one site only (South Pole, SP-G in figure 3), the apparent trend continues as data become available at McMurdo (MM-S from 1986) and Marambio (MA-S from 1988). Considering only the more abundant and better distributed data after 1990, a slightly higher trend of $+0.58 \pm 0.29$ nmol mol^{-1} per decade can be considered, with very high certainty, more representative of the overall Antarctic region. Kumar *et al.* [61] found a positive ozone trend about a factor of 2 higher (approx. 1 nmol mol^{-1} per decade), which may reflect the time period on which their analysis is focused. Most of their data are from the late 1990s and early 2000: our analysis (figure 4, table 1) suggests that the increase in Antarctic ozone was indeed weaker after 2000 with a reduced positive trend of $+0.24 \pm 0.27$ nmol mol^{-1} per decade (with medium certainty).

Ozone in the Arctic shows higher variability between sites than the Antarctic (figure 3); the almost flat trend ($+0.05 \pm 0.24$ nmol mol^{-1} per decade) calculated from the beginning of measurements at Barrow in the late 1970s is consistent with the findings by Helmig *et al.* [20] but has very low certainty and cannot be considered representative of the whole region. By contrast, the downward trend since 2000 (-0.58 ± 0.54 nmol mol^{-1} per decade) is highly certain and coincides with an equivalent decrease in the North Atlantic, as discussed below. These results are consistent with other studies [26,40,60] which noted general decreases in Arctic tropospheric ozone in the last two decades (see also supplementary material, table S4).

(ii) Mid-latitudes

The mean trend over the North Atlantic is positive, reversing to a negative trend after the late 1990s, likely connected to a similar negative trend observed in the Arctic (table 1). Although these trends have very low certainty—largely because different sites show contrasting behaviours (figure 3; supplementary material, table S4)—they are broadly consistent with Gulev *et al.* [62], who suggested with medium certainty that the ozone trend in the Northern Hemisphere (including over continents) has increased by 30–70% since the mid-twentieth century, but also noted the levelling off and reversal in surface ozone over North America and Europe between 1970 and 2010, mostly owing to decreasing anthropogenic emissions of NO_x and reactive carbon from the Northern mid/high latitude regions [63]. By contrast, the North Pacific shows consistent negative trends of about -1 nmol mol^{-1} per decade, despite increased emissions of ozone precursors in East Asia during the period [64], but only with low certainty ($p > 0.1$).

Ozone trends over Southern mid-latitude oceans are generally positive, with the greatest certainty in the South Pacific, where the trend is $+0.53 \pm 0.61$ nmol mol^{-1} per decade since 1990 and $+0.27 \pm 0.33$ nmol mol^{-1} per decade since 2000 (with medium certainty). Inclusion of additional data sources in this region has minimal effect on the calculated values, but the trends have higher certainty (table 1). Conversely, the ozone trend in the South Atlantic is near zero when taking into account the whole time series and becomes positive after 2000, albeit with low certainty. Ozone in the South Indian Ocean shows an increase of $+2.06 \pm 0.36$ nmol mol^{-1} per decade since 1995, which becomes $+1.68 \pm 0.34$ nmol mol^{-1} per decade if short term data from mobile platforms are included (table 1). Although these trends have very high certainty ($p < 0.01$), they cannot be considered representative of the whole region: ozonesondes launches from Reunion are the only long-term source of data in the South Indian Ocean [65], and the observed increases have been linked to changing circulation patterns over Southern Africa and Reunion [66].

(iii) Tropics

Ozone trends in the tropics can only be determined with low and very low certainty ($p > 0.1$), although trends at individual sites are consistent with the regional mean (figure 3; supplementary material, table S4). In the tropical Atlantic, we observe a positive trend of $+0.51 \pm 0.68$ nmol mol^{-1} per decade, which becomes $+1.01 \pm 0.77$ nmol mol^{-1} per decade if all datasets are taken into

Downloaded from royalsocietypublishing.org/rsta/article-pdf/doi/10.1098/rsta.2025.0269/6174177/rsta.2025.0269.pdf
by German Aerospace Centre (DLR) user
on 27 October 2026

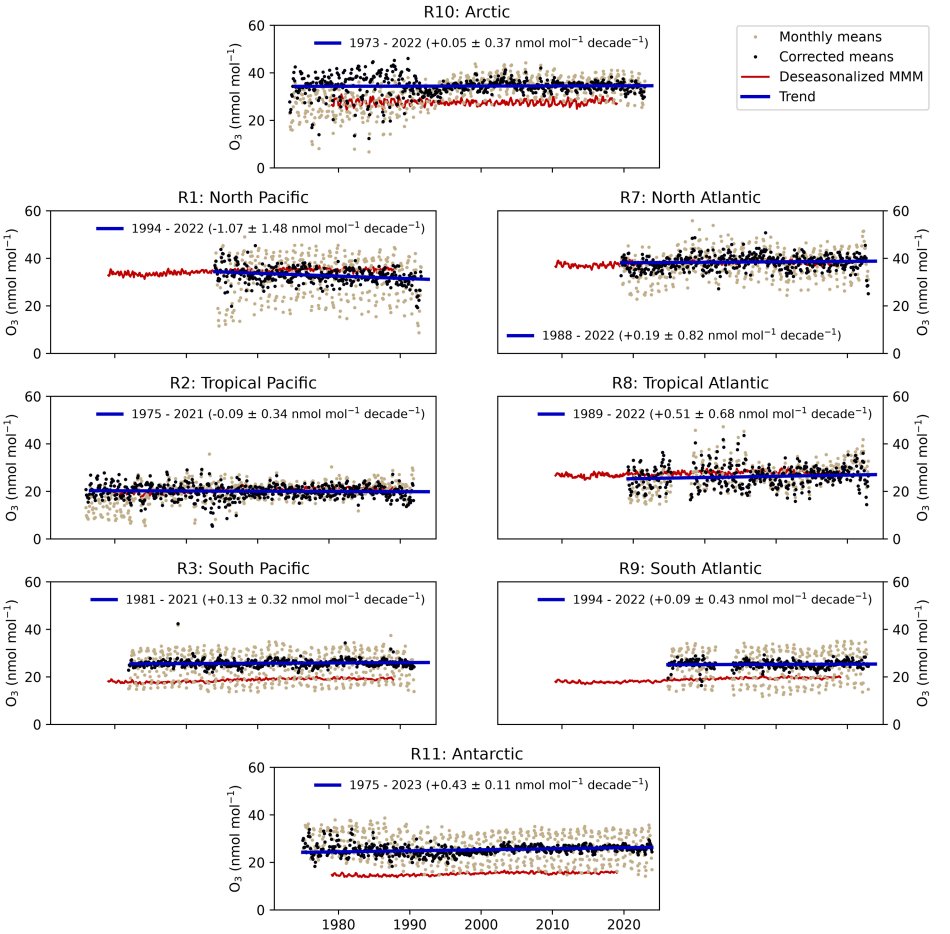


Figure 4. Monthly mean near-surface ozone, with and without adjustments for fitted seasonal (supplementary material, figure S10) and site-specific (figure 3) effects and trends calculated with the LMM method. Data are filtered by the 60-month criterion and trends are calculated from the beginning of the dataset in each region. The trends calculated with data not filtered by the 60-month criterion and starting from different years are shown in the supplementary material (figures S4 and S5).

account (table 1), broadly consistent with those by Thompson *et al.* [65], who only used ozonesonde observations. As mentioned above, unattributed intra-annual variance likely limits the certainty of fitted trends in the tropics. The sharp ozone gradient of the chemical equator is a major contributor to this variance as its location and seasonality vary between years, and it can cause ozone to vary by >100% of the lower values in the tropics (figure 2; supplementary material, figure S2).

Over the tropical Pacific, ozone trends are slightly negative but essentially flat, with very low certainty, even when the 60-month criterion is not applied and all datasets are used (table 1). Cooper *et al.* [60] reported a weak positive trend of 0.2 nmol mol^{-1} per decade with medium certainty, which they concluded to be strongly impacted by increases after 2005. The inclusion of ozonesonde data in our analysis suggests that the coastal measurements at American Samoa [26,65] are an outlier among the long-term datasets, as the overall regional trend since 2000 is instead negative (-0.56 ± 0.50 nmol mol^{-1} per decade), with high certainty. The picture over the tropical Pacific is however complex: both satellite observations [8] [Hubert *et al.*, this issue] and *in situ* observation [67] report positive trends over the Western tropical Pacific, and negative or flat trends over the Eastern tropical Pacific, which suggest that the Pacific region as a whole is not uniform.

Downloaded from royalsocietypublishing.org/rsta/article-pdf/doi/10.1098/rsta.2025.0269/6174177/rsta.2025.0269.pdf
by German Aerospace Centre (DLR) user
on 27 October 2026

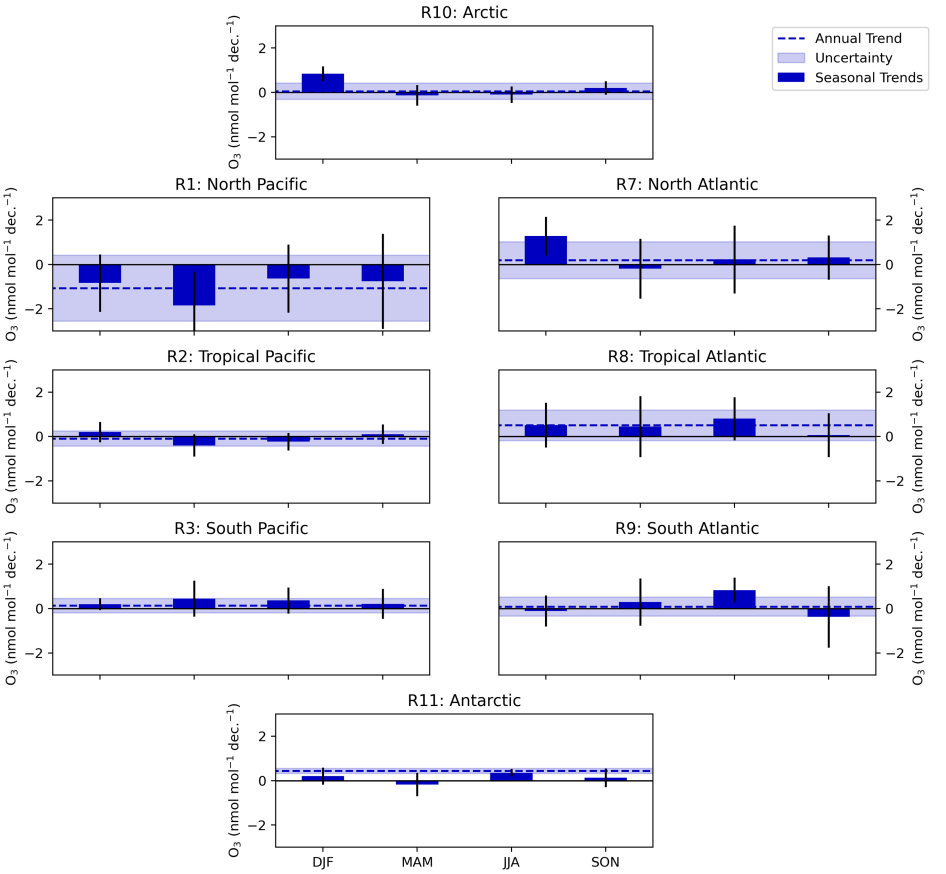


Figure 5. Seasonal ozone trends calculated with the LMM method. Data are filtered by the 60-month criterion; the vertical bars are the 2-σ uncertainties of the calculated trends. Only the regions with sufficient spatio-temporal coverage are shown. The trends calculated starting from different years are shown in the supplementary material (figure S9).

(c) Seasonality of ozone trends

The ozone trends in figure 4 and table 1 are calculated using deseasonalized data, as explained above. In this section, we examine how ozone trends are affected by seasonal patterns. The data were aggregated by season in each region, and the trends were recalculated using the same LMM methodology described above. The results are shown in figure 5 for the whole dataset, compared to overall annual trends, and in figure S9 in the supplementary material for different starting years. In most regions, seasonal trends have larger uncertainties, reflecting less input data, but are not significantly different from the annual trends. However, in some regions, it is apparent that the annual trend is largely driven by a single season, while in others, it emerges from opposing seasonal patterns.

(i) Polar regions

In the Antarctic, we observe a consistent seasonal trend of increasing ozone during the Southern winter (JJA), while changes during the Southern summer (DJF) are almost zero (figure 5). Unique among regions, the Antarctic seasonal trends are systematically lower than the overall trend, driven in part by atypical seasonality at the South Pole. In broad terms, the Arctic mirrors the Antarctic, with increases in the annual ozone maximum during the Northern winter being significantly positive and greater than the annual average trend (figure 5). Increases in Arctic winter

Downloaded from royalsocietypublishing.org/rsta/article-pdf/doi/10.1098/rsta.2025.0269/6174177/rsta.2025.0269.pdf
by German Aerospace Centre (DLR) user
on 27 October 2026

ozone have been previously inferred to reflect decreased titration by anthropogenic NO_x emissions from the Northern Hemisphere temperate zone [68]. The strong seasonal trend during the Arctic spring (MAM), which is especially apparent after 2000 (supplementary material, figure S9), is at least partly connected to the occurrence of ODEs. While the precise timing of ODEs varies by location, both global models and empirical observations indicate that they are related to salinity transfer on young sea ice and particular meteorological conditions, as well as to oceanic halogen emissions [47,69–72].

On a regional scale, our analysis cannot distinguish between changes in frequency, extent or intensity of ODEs, although available evidence suggests that at least the frequency and extent have increased in recent years and are related to atmospheric transport from the mid-latitudes [68]. Similar ODEs are observed over the Antarctic, including at regional scale [73], but our analysis does not indicate that they drive the overall negative trends in the region. Gong *et al.* [47] found that Northern boreal fires lead to an enhancement in Arctic ozone during the Northern summer, but more in the free troposphere than at the surface level: indeed, we observe muted trends in summertime surface ozone (figure 5), consistent with this being more of a free tropospheric phenomenon.

(ii) Mid-latitudes

Seasonal trends in the mid-latitudes show the same increases in wintertime ozone as the adjacent polar regions over the Atlantic but not over the Pacific (figure 5). Positive trends in the North Atlantic wintertime (DJF) ozone likely reflect reduced NO_x emissions in both North America and Europe [74,75], but no such increase in winter ozone is found over the Pacific, despite similar NO_x trends occurring in East Asia [76]. The reason for this difference between the two oceanic basins is unclear, although also apparent by satellite analysis [Hubert *et al.*, this issue].

There is a clear negative trend in North Pacific ozone during the Northern spring (MAM), which is also observed over the North Atlantic (figure 5; supplementary material, figure S9), and corresponds to the annual ozone maximum (supplementary material, figure S1). This may be related to changes in emissions from East Asia [77] and/or STE [Keeble *et al.*, this issue]. Seasonal trends being largest in magnitude across the Pacific (including the tropics) in MAM, but having opposing directions, might plausibly reflect a systemic shift in the chemical equator and be tied to the El Niño–Southern Oscillation (ENSO).

The seasonal cycle of ozone in the South Atlantic does not mirror that of temperate Northern latitudes, peaking instead in the Southern winter (figure 2; supplementary material, figure S10). The largest changes are seen over longer periods of time and are more apparent when using earlier data. Simulating the seasonal cycle at Cape Grim (South Pacific) has shown that increases in VOC ozone precursors, particularly CH_4, can increase the magnitude of the ozone seasonal cycle especially in summertime [78]. Similar changes in CH_4 levels over the South Atlantic and Antarctic might explain increased wintertime ozone.

(iii) Tropics

The ozone trends in different seasons in the tropics show different behaviour over the Atlantic and Pacific. The most positive trends are observed over the tropical Atlantic in JJA, and over the tropical Pacific in DJF. As noted above, tropical ozone over both basins does not show strong seasonality despite rapid changes at individual sites occurring with variable timing from year to year—at least partly related to the position of the chemical equator and, therefore, of the ITCZ (supplementary material, figure S2).

Over the Pacific, the fitted trends are small but potentially consistent across hemispheres with a long-term shift in the chemical equator. However, the latitudinal and seasonal distribution of the observations in the Pacific and Atlantic is not consistent (figure 1), which may imply a sampling bias in our data, so care must be taken not to over-interpret these divergent trends.

Downloaded from royalsocietypublishing.org/rsta/article-pdf/doi/10.1098/rsta.2025.0269/6174177/rsta.2025.0269.pdf
by German Aerospace Centre (DLR) user
on 27 October 2026

(d) Comparison with other trends

The trends shown in figure 1 and figure S4 in the supplementary material include only data below 2 km; absent active convection, this includes the whole marine boundary layer—typically between a few hundred metres to just over 1 km—and we have previously noted the agreement between co-located surface and sonde measurements [25,47]. However, such agreement holds less well for all low altitude observations, and prior work has highlighted that trends can be quite different at different altitudes both at individual sites and regionally [61,79]. Even using only ozonesondes data from Ascension, the trend between 300 and 700 mbar and the trend below 2 km disagree in sign [26]. Likewise, surface and ozonesonde measurements at American Samoa show inconsistent trends with opposite signs (supplementary material, table S4).

Studies using only ship-borne data in the Atlantic from 1977 to 2002 [80] found ozone trends more than a factor of 2 higher than those calculated from contemporary ground sites and in our analysis. We similarly find that the magnitude of trends is greater when including shorter datasets and measurements far from coastal sites and ozonesonde launch locations (table 1). It is possible that ozone over the open ocean behaves differently than at even remote coastal locations, but we lack high quality continuous measurements from the remote ocean to determine this definitively.

Similar to our findings (figure 4), ozonesonde measurements from tropical launch sites indicate weak positive increases in the periods 1998–2019 [81] and 1998–2023 [65], but at several locations, ozone increases are lower, possibly owing to undiagnosed COVID impacts. Comparing our bootstrap LMM analysis for 2000–2022 (supplementary material, table S4) with the Quantile Regression analysis of ozonesondes data at low altitudes [26], we find that most sites agree within the respective uncertainties, showing decreases in ozone at Northern mid-latitudes and more muted trends, varying in sign between the Atlantic and Pacific in the tropics and the Southern mid-latitudes.

5. Discussion

The distribution of ozone in oceanic and polar regions, and its trends over recent decades, is linked to complex changes in its sources and sinks, its precursors and their transport. While global models can help disentangle some of these processes, a definitive attribution of the observed concentrations and trends to specific processes is beyond the scope of this assessment, not least because of the differences between the models, and between the models and the observations (figure 2). In this section, we outline the state of knowledge and examine potential factors impacting the observed trends.

We used simulations from four global models—CHASER, CAM-Chem, EMAC and GISS-E2.1—to investigate long-term changes of the ozone budget over coastal and open ocean regions through analysis of the Net Chemical Change (NCC = production—loss). The NCC was calculated for the period 1980–2018 and averaged across the oceanic and polar regions (supplementary material, table S5). Analysis of the NCC trends reveals both robust signals and substantial inter-model variability, which is used to supplement our review of the key processes that are affecting ozone trends in these regions.

(a) Sources and sinks

The growth of CH_4 levels since the 1980s, largely driven by anthropogenic activity, is widely assumed to be responsible for recent global ozone increases [82–84], and increased NCC in most regions since the 1980s is attributed primarily to this factor. The largest increase in NCC is over the tropical oceans where models agree on the dominant role of CH_4. Observational constraints and large discrepancies between models (figure 2), however, limit our ability to discuss the relative impact of various ozone sources and sinks with confidence. As mentioned above, the

Downloaded from royalsocietypublishing.org/rsta/article-pdf/doi/10.1098/rsta.2025.0269/6174177/rsta.2025.0269.pdf
by German Aerospace Centre (DLR) user
on 27 October 2026

tropics show the largest inter-model spread, with some models indicating strong positive trends (e.g. GISS-E2.1 in the Indian Ocean and Tropical Atlantic), while others simulate flat or negative NCC trends (supplementary material, table S5). These discrepancies reflect differing treatments of physico-chemical processes across models. In the Southern Hemisphere, mid-latitude oceans exhibit small NCC values and weak trends, consistent with low chemical activity and precursor availability. Stable oxygen isotope analysis suggests the chemical drivers of ozone differ significantly between the hemispheres transitioning across the tropics [85], which is qualitatively consistent with our NCC analysis.

Shipping is an important *in situ* source of NO_x strongly influencing marine ozone [86,87]. Recent global modelling studies have attributed 3–6 nmol mol^{-1} of ozone to NO_x emissions from shipping [63,88], and 6–12 nmol mol^{-1} ozone in the Northern mid-latitudes. Ship emissions of NO_x have increased until approximately 2018 [89], and emission inventories indicate declining overall emissions owing to policy control measures implemented since. Nalam *et al.* [63] attributed a ground-level ozone trend of +0.5 nmol mol^{-1} per decade to the increase in ship NO_x emissions. This is greater than almost all regional trends we observe (table 1), which suggests a modelling bias, likely owing to the fine spatial resolution necessary to accurately represent the gradual dispersal of shipping plumes [90]. Nonetheless, such a trend is confirmed by satellite observations (see the TOAR-II Satellite Assessment, [Hubert *et al.*, this issue]). Shipping is limited in the Antarctic, but it is increasing along with other human activities [91] and may become more relevant in the future. NO_x is also transported over the oceans from continental sources via long-lived reservoirs. Recent studies suggest that particulate NO_3^- can be reactivated via photolysis relatively efficiently, especially in marine aerosol [92,93]; this process is potentially important, but not well understood, and its role in the distribution of oceanic NO_x and ozone is currently unclear [44].

Another significant factor that can account for some of the discrepancies between models, and between models and measurements (figure 1), is NO_x emissions from lightning, especially in the tropics [94]. However, the vertical distribution of lightning NO_x is such that most of the emissions occur in the tropical upper troposphere [95] and are much smaller and shorter-lived near the surface, resulting in a generally smaller impact on oceanic ozone [96]. Likewise, biomass burning emissions have a small effect on near-surface ozone on a global scale [63,87,95], although episodic and seasonal increases have been attributed to them across the tropics and mid-latitudes, and in all oceans [28,97–100].

Oceanic VOC emissions are much less characterized than those of CH_4 and NO_x and differ in their representation among models, making the attribution of ozone trends to changes in VOC less certain. There is general consensus that: (i) conditions over the oceans are typically NO_x-limited and therefore less sensitive to changes in VOC, and (ii) oceanic sources of VOC are underrepresented in models [101–104]. Continental emissions also contribute, via long-range transport, to the VOC budget over oceans, although most are not easily distinguished from oceanic emissions [105–107].

In the polar regions, NCC values and trends are minimal for all models, in line with observed stability in surface ozone (figure 4), although there is increasing recognition of the role of emissions from local sources on air pollution in the Arctic [108]. For instance, Oltmans *et al.* [109] attributed the reversal of decadal trends in late-summer surface ozone concentrations at Barrow to the growth and decline of emissions from oil extraction activities in Alaska. NO_x emissions from existing Arctic oil and gas infrastructure are known to perturb ozone and bromine chemistry, thus influencing the Arctic surface ozone seasonal cycles at local and regional scales [72,110]. Conversely, far from fresh emission plumes, moderate increases in NO_x concentrations and associated changes in aerosol acidity may enhance the activity of halogens [111,112], thereby offsetting ozone formation.

Deposition to the ocean surface is a major driver for ozone concentrations, despite large uncertainties in its magnitude; estimates vary between one-sixth [113,114] and one-third [18,115] of total ozone dry deposition globally. Observations indicate that ozone destruction over the oceans is governed by a different paradigm than in polar regions and that, except for titration

Downloaded from royalsocietypublishing.org/rsta/article-pdf/doi/10.1098/rsta.2025.0269/6174177/rsta.2025.0269.pdf
by German Aerospace Centre (DLR) user
on 27 October 2026

by local NO emissions, near-zero ozone is not observed over the oceans [25]. Inorganic iodine is understood to play a key role in controlling deposition velocities [116–118]; in turn, ozone deposition is understood to drive the emission of gas-phase iodine and oxygenated VOCs [119]. This negative feedback [120] could be buffering ozone changes near the ocean surface, explaining the almost flat oceanic trends (figure 4). Ice-core and tree-ring records indicate increased oceanic fluxes of iodine in the Arctic [121] and Northern mid-latitudes [122,123], but not in the Antarctic [70], which is attributed to retreating sea ice and the deposition feedback [120]. This mechanism is likely to have mitigated ozone increases since the 1950s rather than lead to any outright decrease [30]. Coordinated measurements of sea-surface composition, gas-phase concentrations and deposition velocities are currently extremely limited, thus preventing a more accurate assessment of oceanic dry deposition.

(b) Dynamics

As well as emissions of precursor gases and dry deposition, transport processes, such as STE, and large-scale patterns of climate variability, such as ENSO, also impact ozone. STE has been demonstrated to contribute to increased near-surface ozone at least episodically in coastal regions [124–126], and descending ozone lamina have been observed over the ocean [127,128]. Direct observation of stratospheric-derived ozone over the ocean surface has not been made and may be rare, but isentropic transport from the subtropical jet can lead to the tropical surface and, given other observations, likely contributes. For an in-depth discussion of STE more generally, see the TOAR-II STE Assessment [Keeble *et al.*, this issue].

ENSO is one of the leading modes of climate variability: it can impact ozone over the oceans globally via teleconnections, both directly and indirectly, by modulating STE owing to changes in meteorology, ocean temperatures, ozone precursors (e.g. NO_x) and long-range transport of ozone [129,130]. In the Pacific, El Niño events are associated with decreased levels of ozone in the tropics and increases at mid- and high latitudes, largely owing to enhanced advection and mixing. Additionally, Yeh *et al.* [131] suggest that the impact of ENSO on tropospheric ozone over the Pacific, Atlantic and Indian oceans is more significant than previously thought especially in MAM of the following year [132]. The future climate response of ENSO is highly uncertain [133], as is the persistence of existing teleconnections.

Changes in tropical convection and the position of the ITCZ may have influenced regional ozone trends, shifting the strong latitudinal gradient in tropical ozone and the chemical equator (supplementary material, figure S2). The Atlantic ITCZ has shown a northward shift [134], while the Pacific ITCZ has shown a poleward shift [135,136]. As our analysis assumes a consistent seasonal cycle across years and sites, it is uncertain whether these changes are captured. Examination of individual sites does indicate possible site-specific shifts in tropical ozone seasonality. As noted above, the tropics are also the region where there is greatest disagreement among models, which struggle to capture the location of the chemical equator. Any attempt to leverage models to address data coverage issues in the tropics will require better representation of the chemical equator than currently available.

6. Conclusions and outlook

In this assessment, we reviewed the climatology of near surface ozone over 11 oceanic and polar regions using the most extensive dataset of observations from ships, buoys, aircraft and ozonesondes yet assembled, complemented with selected coastal and polar ground sites [25]. The observations show high ozone levels in the Northern Hemisphere and a steep trans-hemispheric gradient, as well as clear seasonal cycles characterized by springtime maxima and summertime minima. However, some regions remain severely undersampled, especially in the Southern Hemisphere.

Downloaded from royalsocietypublishing.org/rsta/article-pdf/doi/10.1098/rsta.2025.0269/6174177/rsta.2025.0269.pdf
by German Aerospace Centre (DLR) user
on 27 October 2026

Long-term ozone trends were calculated using Linear Mixed-effects Modelling (LMM) for nine of the 11 regions with sufficient data coverage. Positive overall trends were found in seven regions, although in almost all cases with low or very low certainty. Of particular note, the longest fitted trends indicate increases in ozone in polar regions and mid-latitude Atlantic during the respective hemispheric winters with high certainty. The regional trend in the Arctic is largely driven by decreases in recent years, especially during spring and summer, resulting in an overall negative trend since 2000. The most persistent negative trends are in the North and Tropical Pacific, with both regions showing particular decreases during the Northern spring.

Drawing on more extensive data, trends calculated from 2000 have low certainty or better across all analysed regions, with four regions showing negative overall trends in more recent years. For 2000–2023, our LMM-based trend methodology is in good agreement with two other studies [26,65] that used a different statistical method with some of the same ground-based and ozonesonde data. Inconsistent seasonal cycles present a limitation on the current LMM implementation, which could be addressed in future work by including site-specific seasonal terms; this, however, requires careful consideration about seasonal data availability and representativeness. Models could aid in filling the data coverage limitation, but, as highlighted here, all models struggle to reproduce intraregional variability. Therefore, there is not a ready alternative to collecting additional data to constrain models, which might then be employed retrospectively.

This assessment does not attempt to attribute the calculated trends to specific processes, but it does compare the observations to six models, and it examines the Net Chemical Change (NCC) in four of these to review the state of knowledge of the main ozone drivers in oceanic and polar regions. Broadly speaking, there is a lack of agreement among the models, and between the models and the observations: most models are able to capture the seasonal variability of ozone, but tend to overestimate it in the Northern Hemisphere and underestimate it in the Southern Hemisphere. While additional process-level investigations are needed to improve our understanding, the greatest issue is a scarcity of direct field observations of ozone and its precursors, which leaves the models insufficiently constrained and limits our ability to assess the representativeness of long-term observations for their broader regions.

Data accessibility. The dataset used in this assessment is described in [25] and available at http://doi.org/10.17596/0004044. Further, datasets provided by MESSy via the DKRZ data pool (https://www.wdc-climate.de/ui/entry?acronym=ESCiMo2_RD1) were used. Supplementary material is available online [137].

Declaration of AI use. We have not used AI-assisted technologies in creating this article.

Authors' contributions. R.S.: conceptualization, investigation, methodology, project administration, supervision, writing—original draft, writing—review and editing; T.K.K.: conceptualization, data curation, formal analysis, investigation, methodology, software, visualization, writing—original draft, writing—review and editing; T.S.: formal analysis, investigation, methodology, visualization, writing—original draft, writing—review and editing; A.B.: formal analysis, investigation, methodology, writing—original draft, writing—review and editing; Y.K.: conceptualization, data curation, investigation, methodology, project administration, supervision, writing—original draft, writing—review and editing; A.M.: data curation, investigation, methodology, software, visualization, writing—original draft, writing—review and editing; M.P.: writing—original draft, writing—review and editing; K.A.R.: investigation, methodology, writing—original draft, writing—review and editing; M.J.R.: data curation, formal analysis, investigation, methodology, software, writing—original draft, writing—review and editing; M.R.R.: investigation, methodology, writing—original draft, writing—review and editing; N.L.A.: formal analysis, writing—review and editing; J.A.A.: writing—original draft, writing—review and editing; K.-L.C.: data curation, formal analysis, investigation, methodology, software, writing—review and editing; J.H.C.: formal analysis, writing—review and editing; W.G.: visualization, writing—review and editing; F.I.-S.: formal analysis, investigation, methodology, writing—original draft, writing—review and editing; U.I.: formal analysis, writing—original draft, writing—review and editing; P.J: formal analysis, writing—review and editing; D.E.K.: visualization, writing—review and editing; M.M.: formal analysis, writing—original draft, writing—review and editing; R.M.: writing—original draft, writing—review and editing; R.M.S.: writing—review and editing; A.M.T.: writing—review and editing; K.T.: writing—review and editing; A.S.-L.: conceptualization, investigation, project administration, supervision, writing—original draft, writing—review and editing.

Downloaded from royalsocietypublishing.org/rsta/article-pdf/doi/10.1098/rsta.2025.0269/6174177/rsta.2025.0269.pdf
by German Aerospace Centre (DLR) user
on 27 October 2026

All authors gave final approval for publication and agreed to be held accountable for the work performed therein.

Conflict of interest declaration. We declare we have no competing interests.

Funding. Theodore Koenig acknowledges support from the Hong Kong Environment and Conservation Fund (ECF 2023-102). Alfonso Saiz-Lopez, Alba Badia and Fernando Iglesias-Suarez acknowledge support from the CLIMAHAL project (ERC-2016-COG 726349), funded by the European Research Council Executive Agency under the European Union's Horizon 2020. They would also like to thank the CESM project, which is supported primarily by the NSF, led by the National Centre for Atmospheric Research (NCAR), which is a major facility sponsored by the NSF under cooperative agreement 1852977. Takashi Sekiya and Yugo Kanaya acknowledge support by the KAKENHI grant no. 21H04933. Yugo Kanaya acknowledges support from the Arctic Challenge for Sustainability 3 (ArCS-3), Program grant no. JPMXD1720251001 of the Ministry of Education, Culture, Sports, Science, and Technology, and from the Specified Critical Technologies Research Promotion grants from the Cabinet Office, Government of Japan. Marios Panagi acknowledges support from the EMME-CARE project, funded by the European Union's Horizon 2020 Research and Innovation Programme (grant agreement no. 856612, with co-funding from the Government of Cyprus), and to the EU project AVENGERS (grant agreement no. 101081322). Katie Read is funded by the Natural Environment Research Council (NERC) through the National Centre for Atmospheric Science (NCAS). Maria Russo and Nathan Luke Abraham used Monsoon2 to perform the UKESM simulations, a collaborative High-Performance Computing facility funded by the Met Office and the UK Natural Environment Research Council (NERC), and JASMIN, the UK collaborative data analysis facility. They would also like to thank NERC for financial support through the VISION project, NE/Z503393/1. Kai-Lan Chang is supported by NOAA Cooperative Agreement NA22OAR4320151. Ulas Im acknowledges the European Union's Horizon Europe programme funded project CleanCloud (no. 101137639). Debra Kollonige, Ryan Stauffer and Anne Thompson are supported by NASA Headquarters program on Upper Atmosphere Composition Observations. Mariano Mertens is supported by the German Federal Ministry of Research, Technology and Space (funding no. 01LN2207A, IMPAC2T). The work involving the EMAC model used resources of the Deutsches Klimarechenzentrum (DKRZ) granted by its Scientific Steering Committee (WLA) under project ID id0853. Raeesa Moolla acknowledges funding support from Stellenbosch University and DHET FPP (Phase 01) grant programme.

Acknowledgements. The authors acknowledge guidance and support from the International Global Atmospheric Chemistry (IGAC) project. Tropospheric Ozone Assessment Report II (TOAR-II) has been conducted as a sponsored IGAC Activity. This work utilized computing resources, technical support and data storage provided by the Climate Simulation Laboratory within NCAR's Computational and Information Systems Laboratory, sponsored by the NSF. The work involving the EMAC model used resources of the Deutsches Klimarechenzentrum (DKRZ) granted by its Scientific Steering Committee (WLA) under project ID id0853. Ulas Im acknowledges the EuroHPC Joint Undertaking for awarding this project access to the EuroHPC supercomputer LUMI, hosted by CSC (Finland) and the LUMI consortium through a EuroHPC Regular Access call. Roberto Sommariva thanks Bill Bloss and Christian Pfrang (University of Birmingham, UK) for their support during this project.

References

1. Forster P *et al*. 2021 The Earth's energy budget, climate feedbacks, and climate sensitivity. In *Climate change 2021: the physical science basis. Contribution of working group I to the sixth assessment report of the Intergovernmental Panel on Climate Change*, pp. 923–1054. Cambridge, UK: Cambridge University Press.
2. Jacob DJ, Winner DA. 2009 Effect of climate change on air quality. *Atmos. Environ.* **43**, 51–63. (doi:10.1016/j.atmosenv.2008.09.051)
3. Monks PS *et al*. 2015 Tropospheric ozone and its precursors from the urban to the global scale from air quality to short-lived climate forcer. *Atmos. Chem. Phys.* **15**, 8889–8973. (doi:10.5194/acp-15-8889-2015)
4. Archibald AT *et al*. 2020 Tropospheric Ozone Assessment Report: a critical review of changes in the tropospheric ozone burden and budget from 1850 to 2100. *Elem. Sci. Anth.* **8**, 1. (doi:10.1525/elementa.2020.034)
5. Szopa S *et al*. 2023 Short-lived climate forcers. In *Climate change 2021: the physical science basis. Contribution of working group I to the sixth assessment report of the Intergovernmental Panel on Climate Change*, pp. 817–922. Cambridge, UK: Cambridge University Press.

Downloaded from royalsocietypublishing.org/rsta/article-pdf/doi/10.1098/rsta.2025.0269/6174177/rsta.2025.0269.pdf
by German Aerospace Centre (DLR) user
on 27 October 2026

6. Young PJ *et al*. 2013 Pre-industrial to end 21st century projections of tropospheric ozone from the atmospheric chemistry and climate model intercomparison project (ACCMIP). *Atmos. Chem. Phys.* **13**, 2063–2090. (doi:10.5194/acp-13-2063-2013)
7. Cooper OR *et al*. 2014 Global distribution and trends of tropospheric ozone: an observation-based review. *Elem. Sci. Anth.* **2**, 000029. (doi:10.12952/journal.elementa.000029)
8. Gaudel A *et al*. 2018 Tropospheric ozone assessment report: present-day distribution and trends of tropospheric ozone relevant to climate and global atmospheric chemistry model evaluation. *Elem. Sci. Anth.* **6**, 39. (doi:10.1525/elementa.291)
9. Wang T, Dai J, Lam KS, Poon CN, Brasseur GP. 2019 Twenty-five years of lower tropospheric ozone observations in tropical East Asia: the influence of emissions and weather patterns. *Geophys. Res. Lett.* **46**, 11 463–11 470. (doi:10.1029/2019GL084459)
10. Xu F, Hu K, Lu SH, Guo S, Wu YC, Xie Y, Zhang HH, Hu M. 2025 Enhanced marine VOC emissions driven by terrestrial nutrient inputs and their impact on urban air quality in coastal regions. *Environ. Sci. Technol.* **59**, 8140–8154. (doi:10.1021/acs.est.4c12655)
11. Winkler P. 1988 Surface ozone over the Atlantic ocean. *J. Atmos. Chem*. **7**, 73–91. (doi:10.1007/BF00048255)
12. Saiz-Lopez A, von Glasow R. 2012 Reactive halogen chemistry in the troposphere. *Chem. Soc. Rev.* **41**, 6448–6472. (doi:10.1039/c2cs35208g)
13. Sekiya T, Kanaya Y, Sudo K, Taketani F, Iwamoto Y, Aita MN, Yamamoto A, Kawamoto K. 2020 Global bromine- and iodine-mediated tropospheric ozone loss estimated using the CHASER chemical transport model. *SOLA* **16**, 220–227. (doi:10.2151/sola.2020-037)
14. Simpson WR, Brown SS, Saiz-Lopez A, Thornton JA, von Glasow R. 2015 Tropospheric halogen chemistry: sources, cycling, and impacts. *Chem. Rev.* **115**, 4035–4062. (doi:10.1021/cr5006638)
15. Helmig D, Johnson B, Oltmans SJ, Neff W, Eisele F, Davis D D. 2008 Elevated ozone in the boundary layer at South Pole. *Atmos. Environ.* **42**, 2788–2803. (doi:10.1016/j.atmosenv.2006.12.032)
16. Legrand M, Preunkert S, Jourdain B, Gallée H, Goutail F, Weller R, Savarino J. 2009 Year-round record of surface ozone at coastal (Dumont d'Urville) and inland (Concordia) sites in East Antarctica. *J. Geophys. Res. Atmos.* **114**, D20306. (doi:10.1029/2008JD011667)
17. Zatko M, Geng L, Alexander B, Sofen E, Klein K. 2016 The impact of snow nitrate photolysis on boundary layer chemistry and the recycling and redistribution of reactive nitrogen across Antarctica and Greenland in a global chemical transport model. *Atmos. Chem. Phys.* **16**, 2819–2842. (doi:10.5194/acp-16-2819-2016)
18. Ganzeveld L, Helmig D, Fairall CW, Hare J, Pozzer A. 2009 Atmosphere-ocean ozone exchange: a global modeling study of biogeochemical, atmospheric, and waterside turbulence dependencies. *Glob. Biogeochem. Cycles* **23**, GB4021. (doi:10.1029/2008GB003301)
19. Hardacre C, Wild O, Emberson L. 2015 An evaluation of ozone dry deposition in global scale chemistry climate models. *Atmos. Chem. Phys*. **15**, 6419–6436. (doi:10.5194/acp-15-6419-2015)
20. Helmig D, Bocquet F, Cohen L, Oltmans SJ. 2007 Ozone uptake to the polar snowpack at Summit, Greenland. *Atmos. Environ.* **41**, 5061–5076. (doi:10.1016/j.atmosenv.2006.06.064)
21. Barten JGM *et al*. 2023 Low ozone dry deposition rates to sea ice during the MOSAiC field campaign: implications for the Arctic boundary layer ozone budget. *Elem. Sci. Anth.* **11**, 0086. (doi:10.1525/elementa.2022.0 0086)
22. Schultz MG *et al*. 2017 Tropospheric ozone assessment report: database and metrics data of global surface ozone observations. *Elem. Sci. Anth.* **5**, 58. (doi:10.1525/elementa.244)
23. Fleming ZL *et al*. 2018 Tropospheric ozone assessment report: present-day ozone distribution and trends relevant to human health. *Elem. Sci. Anth*. **6**, 12. (doi:10.1525/elementa.273)
24. Mills G *et al*. 2018 Ozone pollution will compromise efforts to increase global wheat production. *Glob. Change Biol*. **24**, 3560–3574. (doi:10.1111/gcb.14157)
25. Kanaya Y *et al*. 2025 Observational ozone data over the global oceans and polar regions: the TOAR-II oceans data set version 2024. *Earth Syst. Sci. Data* **2025**, 1–49. (doi:10.5194/essd-2024-566)
26. Van Malderen R *et al*. 2025 Global ground-based tropospheric ozone measurements: reference data and individual site trends (2000–2022) from the TOAR-II/HEGIFTOM project. *Atmos. Chem. Phys.* **25**, 7187–7225. (doi:10.5194/acp-25-7187-2025)

Downloaded from royalsocietypublishing.org/rsta/article-pdf/doi/10.1098/rsta.2025.0269/6174177/rsta.2025.0269.pdf
by German Aerospace Centre (DLR) user
on 27 October 2026

27. Gaudel A *et al*. 2024 Tropical tropospheric ozone distribution and trends from in situ and satellite data. *Atmos. Chem. Phys*. **24**, 9975–10 000. (doi:10.5194/acp-24-9975-2024)
28. Okamoto S, Cuesta J, Dufour G, Eremenko M, Miyazaki K, Boonne C, Tanimoto H, Peischl J, Thompson C. 2026 Natural and anthropogenic influence on tropospheric ozone variability over the tropical atlantic unveiled by satellite, reanalyses and *in situ* observations. *Atmos. Chem. Phys.* **26**, 4685–4709. (doi:10.5194/acp-26-4685-2026)
29. Badia A *et al*. 2021 The role of natural halogens in global tropospheric ozone chemistry and budget under different 21st century climate scenarios. *J. Geophys. Res. Atmos*. **126**, e2021JD034859. (doi:10.1029/2021JD034859)
30. Iglesias-Suarez F *et al*. 2020 Natural halogens buffer tropospheric ozone in a changing climate. *Nat. Clim. Change* **10**, 147–154. (doi:10.1038/s41558-019-0675-6)
31. Sellar AA *et al*. 2019 UKESM1: description and evaluation of the U.K. earth system model. *J. Adv. Model. Earth Syst*. **11**, 4513–4558. (doi:10.1029/2019MS001739)
32. Archibald AT *et al*. 2020 Description and evaluation of the UKCA stratosphere–troposphere chemistry scheme (StratTrop vn 1.0) implemented in UKESM1. *Geosci. Model Dev.* **13**, 1223–1266. (doi:10.5194/gmd-13-1223-2020)
33. Jöckel P *et al*. 2016 Earth system chemistry integrated modelling (ESCiMo) with the modular earth submodel system (MESSy) version 2.51. *Geosci. Model Dev.* **9**, 1153–1200. (doi:10.5194/gmd-9-1153-2016)
34. Kelley M *et al*. 2020 GISS-E2.1: configurations and climatology. *J. Adv. Model. Earth Syst.* **12**, e2019MS002025. (doi:10.1029/2019MS002025)
35. Im U *et al*. 2021 Present and future aerosol impacts on arctic climate change in the GISS-E2.1 earth system model. *Atmos. Chem. Phys.* **21**, 10 413–10 438. (doi:10.5194/acp-21-10413-2021)
36. Christensen JH. 1997 The Danish Eulerian hemispheric model — a three-dimensional air pollution model used for the arctic. *Atmos. Environ.* **31**, 4169–4191. (doi:10.1016/S1352-2310(97)00264-1)
37. Brandt J *et al*. 2012 An integrated model study for Europe and North America using the Danish Eulerian Hemispheric Model with focus on intercontinental transport of air pollution. *Atmos. Environ.* **53**, 156–176. (doi:10.1016/j.atmosenv.2012.01.011)
38. Saiz-Lopez A *et al*. 2023 Natural short-lived halogens exert an indirect cooling effect on climate. *Nature* **618**, 967–973. (doi:10.1038/s41586-023-06119-z)
39. Saiz-Lopez A *et al*. 2025 The influence of short-lived halogens on atmospheric chemistry and climate. *Nature* **648**, 289–299. (doi:10.1038/s41586-025-09753-x)
40. Elshorbany Y *et al*. 2024 Tropospheric ozone precursors: global and regional distributions, trends, and variability. *Atmos. Chem. Phys.* **24**, 12 225–12 257. (doi:10.5194/acp-24-12225-2024)
41. Hamilton JF *et al*. 2008 Observations of an atmospheric chemical equator and its implications for the tropical warm pool region. *J. Geophys. Res. Atmos*. **113**, D20313. (doi:10.1029/2008JD009940)
42. Barten JGM, Ganzeveld LN, Steeneveld GJ, Krol MC. 2021 Role of oceanic ozone deposition in explaining temporal variability in surface ozone at high arctic sites. *Atmos. Chem. Phys*. **21**, 10 229–10 248. (doi:10.5194/acp-21-10229-2021)
43. Lin H *et al*. 2024 Intercomparison of GEOS-Chem and CAM-chem tropospheric oxidant chemistry within the community earth system model version 2 (CESM2). *Atmos. Chem. Phys*. **24**, 8607–8624. (doi:10.5194/acp-24-8607-2024)
44. Rowlinson MJ *et al*. 2025 A nitrate photolysis source of tropospheric HONO is incompatible with current understanding of atmospheric chemistry. *Atmos. Chem. Phys*. **25**, 16 945–16 968. (doi:10.5194/acp-25-16945-2025)
45. Whaley CH *et al*. 2023 Arctic tropospheric ozone: assessment of current knowledge and model performance. *Atmos. Chem. Phys*. **23**, 637–661. (doi:10.5194/acp-23-637-2023)
46. Fernandez RP *et al*. 2024 Arctic halogens reduce ozone in the northern mid-latitudes. *Proc. Natl Acad. Sci. USA* **121**, e2401975121. (doi:10.1073/pnas.2401975121)
47. Gong W *et al*. 2025 Modelling arctic lower tropospheric ozone: processes controlling seasonal variations. *Atmos. Chem. Phys.* **25**, 8355–8405. (doi:10.5194/acp-25-8355-2025)
48. Custard KD, Raso ARW, Shepson PB, Staebler RM, Pratt KA. 2017 Production and release of molecular bromine and chlorine from the arctic coastal snowpack. *ACS Earth Space Chem.* **1**, 142–151. (doi:10.1021/acsearthspacechem.7b00014)

Downloaded from royalsocietypublishing.org/rsta/article-pdf/doi/10.1098/rsta.2025.0269/6174177/rsta.2025.0269.pdf
by German Aerospace Centre (DLR) user
on 27 October 2026

49. Pratt KA *et al*. 2013 Photochemical production of molecular bromine in arctic surface snowpacks. *Nat. Geosci.* **6**, 351–356. (doi:10.1038/ngeo1779)
50. Jones AE, Anderson PS, Begoin M, Brough N, Hutterli MA, Marshall GJ, Richter A, Roscoe HK, Wolff EW. 2009 BrO, blizzards, and drivers of polar tropospheric ozone depletion events. *Atmos. Chem. Phys.* **9**, 4639–4652. (doi:10.5194/acp-9-4639-2009)
51. Yang X, Pyle JA, Cox RA. 2008 Sea salt aerosol production and bromine release: role of snow on sea ice. *Geophys. Res. Lett.* **35**, L16815. (doi:10.1029/2008GL034536)
52. Fan SM, Jacob DJ. 1992 Surface ozone depletion in arctic spring sustained by bromine reactions on aerosols. *Nature* **359**, 522–524. (doi:10.1038/359522a0)
53. Michalowski BA, Francisco JS, Li SM, Barrie LA, Bottenheim JW, Shepson PB. 2000 A computer model study of multiphase chemistry in the arctic boundary layer during polar sunrise. *J. Geophys. Res. Atmos.* **105**, 15 131–15 145. (doi:10.1029/2000JD900004)
54. Peterson PK *et al*. 2017 Observations of bromine monoxide transport in the arctic sustained on aerosol particles. *Atmos. Chem. Phys.* **17**, 7567–7579. (doi:10.5194/acp-17-7567-2017)
55. Toyota K, McConnell JC, Staebler RM, Dastoor AP. 2014 Air–snowpack exchange of bromine, ozone and mercury in the springtime arctic simulated by the 1-D model PHANTAS – part 1: in-snow bromine activation and its impact on ozone. *Atmos. Chem. Phys.* **14**, 4101–4133. (doi:10.5194/acp-14-4101-2014)
56. Chang KL, Schultz MG, Koren G, Selke N. 2023 Guidance note on best statistical practices for TOAR analyses. (doi:10.48550/arXiv.2304.14236)
57. Chang KL *et al*. 2022 Impact of the COVID-19 economic downturn on tropospheric ozone trends: an uncertainty weighted data synthesis for quantifying regional anomalies above Western North America and Europe. *AGU Adv.* **3**, e2021AV000542. (doi:10.1029/2021AV000542)
58. Van Malderen R *et al*. 2025 Ground-based tropospheric ozone measurements: regional tropospheric ozone column trends from the TOAR-II/HEGIFTOM homogenized datasets. *Atmos. Chem. Phys.* **25**, 9905–9935. (doi:10.5194/acp-25-9905-2025)
59. Mastrandrea MD *et al*. 2010 Technical Report *Guidance note for lead authors of the IPCC fifth assessment report on consistent treatment of uncertainties*. Geneva, Switzerland: Intergovernmental Panel on Climate Change (IPCC). Available at https://www.ipcc.ch/site/assets/uploads/2017/08/AR5_Uncertainty_Guidance_Note.pdf.
60. Cooper OR *et al*. 2020 Multi-decadal surface ozone trends at globally distributed remote locations. *Elem. Sci. Anth.* **8**, 23. (doi:10.1525/elementa.420)
61. Kumar P *et al*. 2021 The increasing surface ozone and tropospheric ozone in Antarctica and their possible drivers. *Environ. Sci. Technol.* **55**, 8542–8553. (doi:10.1021/acs.est.0c08491)
62. Gulev SK *et al*. 2023 *Changing state of the climate system.* In *Climate change 2021: the physical science basis. Contribution of working group I to the sixth assessment report of the Intergovernmental Panel on Climate Change*, pp. 287–422. Cambridge, UK: Cambridge University Press.
63. Nalam A, Lupaşcu A, Ansari T, Butler T. 2025 Regional and sectoral contributions of NO_x and reactive carbon emission sources to global trends in tropospheric ozone during the 2000–2018 period. *Atmos. Chem. Phys.* **25**, 5287–5311. (doi:10.5194/acp-25-5287-2025)
64. Li B *et al*. 2021 A comprehensive review on anthropogenic volatile organic compounds (VOCs) emission estimates in China: comparison and outlook. *Environ. Int.* **156**, 106710. (doi:10.1016/j.envint.2021.106710)
65. Thompson AM *et al*. 2025 Tropical tropospheric ozone trends (1998 to 2023): new perspectives from SHADOZ, IAGOS and OMI/MLS observations. *Atmos. Chem. Phys.* **25**, 18 475–18 507. (doi:10.5194/acp-25-18475-2025)
66. Millet T *et al*. 2025 Evidence for subtropical dynamical changes in reunion ozone trends (1998-2021). *Earth Space Sci.* **12**, e2025EA004398. (doi:10.1029/2025ea004398)
67. Wang H *et al*. 2022 Global tropospheric ozone trends, attributions, and radiative impacts in 1995–2017: an integrated analysis using aircraft (IAGOS) observations, ozonesonde, and multi-decadal chemical model simulations. *Atmos. Chem. Phys.* **22**, 13 753–13 782. (doi:10.5194/acp-22-13753-2022)
68. Law KS *et al*. 2023 Arctic tropospheric ozone trends. *Geophys. Res. Lett.* **50**, e2023GL103096. (doi:10.1029/2023GL103096)

Downloaded from royalsocietypublishing.org/rsta/article-pdf/doi/10.1098/rsta.2025.0269/6174177/rsta.2025.0269.pdf
by German Aerospace Centre (DLR) user
on 27 October 2026

69. Halfacre JW *et al*. 2014 Temporal and spatial characteristics of ozone depletion events from measurements in the Arctic. *Atmos. Chem. Phys.* **14**, 4875–4894. (doi:10.5194/acp-14-4875-2014)
70. Spolaor A *et al*. 2021 Antarctic ozone hole modifies iodine geochemistry on the Antarctic Plateau. *Nat. Commun.* **12**, 5836. (doi:10.1038/s41467-021-26109-x)
71. Pernov JB, Hjorth JL, Sørensen LL, Skov H. 2024 On the dynamics of ozone depletion events at Villum Research Station in the High Arctic. *Atmos. Chem. Phys.* **24**, 13 603–13 631. (doi:10.5194/acp-24-13603-2024)
72. Widmaier EM, Jensen AR, Pratt KA. 2025 Arctic tropospheric ozone seasonality, depletion, and oil field influence. *Faraday Discuss.* **258**, 265–292. (doi:10.1039/D4FD00166D)
73. Jones AE, Wolff EW, Brough N, Bauguitte SJB, Weller R, Yela M, Navarro-Comas M, Ochoa HA, Theys N. 2013 The spatial scale of ozone depletion events derived from an autonomous surface ozone network in coastal Antarctica. *Atmos. Chem. Phys.* **13**, 1457–1467. (doi:10.5194/acp-13-1457-2013)
74. Jhun I, Coull BA, Zanobetti A, Koutrakis P. 2015 The impact of nitrogen oxides concentration decreases on ozone trends in the USA. *Air Qual. Atmos. Health* **8**, 283–292. (doi:10.1007/s11869-014-0279-2)
75. Bowman H *et al*. 2022 Changes in anthropogenic precursor emissions drive shifts in the ozone seasonal cycle throughout the northern midlatitude troposphere. *Atmos. Chem. Phys.* **22**, 3507–3524. (doi:10.5194/acp-22-3507-2022)
76. Wang T, Xue L, Feng Z, Dai J, Zhang Y, Tan Y. 2022 Ground-level ozone pollution in China: a synthesis of recent findings on influencing factors and impacts. *Environ. Res. Lett.* **17**, 063003. (doi:10.1088/1748-9326/ac69fe)
77. Li K *et al*. 2025 Surface and tropospheric ozone over East Asia and Southeast Asia from observations: distributions, trends, and variability. *Atmos. Chem. Phys.* **25**, 11 575–11 596. (doi:10.5194/acp-25-11575-2025)
78. Pavelin E. 1999 Evaluation of pre-industrial surface ozone measurements made using Schönbein's method. *Atmos. Environ.* **33**, 919–929. (doi:10.1016/S1352-2310(98)00257-X)
79. Stauffer RM, Thompson AM, Oltmans SJ, Johnson BJ. 2017 Tropospheric ozonesonde profiles at long-term U.S. monitoring sites: 2. links between Trinidad Head, CA, profile clusters and inland surface ozone measurements. *J. Geophys. Res. Atmos.* **122**, 1261–1280. (doi:10.1002/2016JD025254)
80. Lelieveld J, van Aardenne J, Fischer H, de Reus M, Williams J, Winkler P. 2004 Increasing ozone over the Atlantic Ocean. *Science* **304**, 1483–1487. (doi:10.1126/science.1096777)
81. Thompson AM, Stauffer RM, Wargan K, Witte JC, Kollonige DE, Ziemke JR. 2021 Regional and seasonal trends in tropical ozone from SHADOZ profiles: reference for models and satellite products. *J. Geophys. Res. Atmos.* **126**, e2021JD034691. (doi:10.1029/2021JD034691)
82. Fiore AM, West JJ, Horowitz LW, Naik V, Schwarzkopf MD. 2008 Characterizing the tropospheric ozone response to methane emission controls and the benefits to climate and air quality. *J. Geophys. Res. Atmos.* **113**, D08307. (doi:10.1029/2007JD009162)
83. Isaksen ISA *et al*. 2014 Atmospheric ozone and methane in a changing climate. *Atmosphere* **5**, 518–535. (doi:10.3390/atmos5030518)
84. Zhang Y, Cooper OR, Gaudel A, Thompson AM, Nédélec P, Ogino SY, West JJ. 2016 Tropospheric ozone change from 1980 to 2010 dominated by equatorward redistribution of emissions. *Nat. Geosci.* **9**, 875–879. (doi:10.1038/ngeo2827)
85. Vicars WC, Savarino J. 2014 Quantitative constraints on the ^{17}O-excess (Δ^{17}O) signature of surface ozone: ambient measurements from 50°N to 50°S using the nitrite-coated filter technique. *Geochim. Cosmochim. Acta* **135**, 270–287. (doi:10.1016/j.gca.2014.03.023)
86. Lawrence MG, Crutzen PJ. 1999 Influence of NO_x emissions from ships on tropospheric photochemistry and climate. *Nature* **402**, 167–170. (doi:10.1038/46013)
87. Butler T, Lupascu A, Nalam A. 2020 Attribution of ground-level ozone to anthropogenic and natural sources of nitrogen oxides and reactive carbon in a global chemical transport model. *Atmos. Chem. Phys.* **20**, 10 707–10 731. (doi:10.5194/acp-20-10707-2020)
88. Mertens M *et al*. 2024 The contribution of transport emissions to ozone mixing ratios and methane lifetime in 2015 and 2050 in the shared socioeconomic pathways (SSPs). *Atmos. Chem. Phys.* **24**, 12 079–12 106. (doi:10.5194/acp-24-12079-2024)

Downloaded from royalsocietypublishing.org/rsta/article-pdf/doi/10.1098/rsta.2025.0269/6174177/rsta.2025.0269.pdf
by German Aerospace Centre (DLR) user
on 27 October 2026

89. Yi W, Wang X, He T, Liu H, Luo Z, Lv Z, He K. 2025 The high-resolution global shipping emission inventory by the Shipping Emission Inventory Model (SEIM). *Earth Syst. Sci. Data.* **17**, 277–292. (doi:10.5194/essd-17-277-2025)
90. Kim HS, Kim YH, Han KM, Kim J, Song CH. 2016 Ozone production efficiency of a ship-plume: ITCT 2K2 case study. *Chemosphere* **143**, 17–23. (doi:10.1016/j.chemosphere.2015.05.022)
91. Ding X, Ai S, Shah SA, Shen Q, Cui M, Pimpirev C, Cai Y. 2025 High-resolution mapping of southern ocean shipping emissions reveals policy-critical hotspots and post-pandemic rebound. *J. Environ. Manag.* **392**, 126738. (doi:10.1016/j.jenvman.2025.126738)
92. Andersen ST *et al*. 2023 Extensive field evidence for the release of HONO from the photolysis of nitrate aerosols. *Sci. Adv.* **9**, eadd6266. (doi:10.1126/sciadv.add6266)
93. Shen H, Li Q, Xu F, Xue L, Hu Y, Saiz-Lopez A, Wang W, Wang T. 2025 Aerosol iodide accelerates reactive nitrogen cycling in the marine atmosphere. *Nat. Commun.* **16**, 8148. (doi:10.1038/s41467-025-63420-3)
94. Bond DW, Steiger S, Zhang R, Tie X, Orville RE. 2002 The importance of NO_x production by lightning in the tropics. *Atmos. Environ.* **36**, 1509–1519. (doi:10.1016/S1352-2310(01)00553-2)
95. Grewe V, Tsati E, Mertens M, Frömming C, Jöckel P. 2017 Contribution of emissions to concentrations: the TAGGING 1.0 submodel based on the modular earth submodel system (MESSy 2.52). *Geosci. Model Dev.* **10**, 2615–2633. (doi:10.5194/gmd-10-2615-2017)
96. Ott LE, Pickering KE, Stenchikov GL, Allen DJ, DeCaria AJ, Ridley B, Lin RF, Lang S, Tao WK. 2010 Production of lightning NO_x and its vertical distribution calculated from three-dimensional cloud-scale chemical transport model simulations. *J. Geophys. Res. Atmos.* **115**, D04301. (doi:10.1029/2009JD011880)
97. Ridder T, Gerbig C, Notholt J, Rex M, Schrems O, Warneke T, Zhang L. 2012 Ship-borne FTIR measurements of CO and O_3 in the Western Pacific from 43°N to 35°S: an evaluation of the sources. *Atmos. Chem. Phys.* **12**, 815–828. (doi:10.5194/acp-12-815-2012)
98. Liu J, Rodriguez JM, Thompson AM, Logan JA, Douglass AR, Olsen MA, Steenrod SD, Posny F. 2016 Origins of tropospheric ozone interannual variation over réunion: a model investigation. *J. Geophys. Res. Atmos.* **121**, 521–537. (doi:10.1002/2015JD023981)
99. Lebourgeois T *et al*. 2024 Seasonal, regional, and vertical characteristics of high-carbon-monoxide plumes along with their associated ozone anomalies, as seen by IAGOS between 2002 and 2019. *Atmos. Chem. Phys.* **24**, 13 975–14 004. (doi:10.5194/acp-24-13975-2024)
100. Xue L *et al*. 2021 ENSO and Southeast Asian biomass burning modulate subtropical trans-Pacific ozone transport. *Natl Sci. Rev.* **8**, nwaa132. (doi:10.1093/nsr/nwaa132)
101. Yu Z, Li Y. 2021 Marine volatile organic compounds and their impacts on marine aerosol—a review. *Sci. Total Environ.* **768**, 145054. (doi:10.1016/j.scitotenv.2021.145054)
102. Zhao D, Yang Y, Tham YJ, Zou S. 2023 Emission of marine volatile organic compounds (VOCs) by phytoplankton—a review. *Mar. Environ. Res.* **191**, 106177. (doi:10.1016/j.marenvres.2023.106177)
103. Ferracci V *et al*. 2024 Atmospheric isoprene measurements reveal larger-than-expected southern ocean emissions. *Nat. Commun.* **15**, 2571. (doi:10.1038/s41467-024-46744-4)
104. Wang J, Li J, Tchinda NT, Du L. 2025 Marine biogenic volatile organic compounds: production, emission, atmospheric transformation, and climate effects. *Curr. Pollut. Rep.* **11**, 37. (doi:10.1007/s40726-025-00365-7)
105. Arnold SR *et al*. 2009 Evaluation of the global oceanic isoprene source and its impacts on marine organic carbon aerosol. *Atmos. Chem. Phys.* **9**, 1253–1262. (doi:10.5194/acp-9-1253-2009)
106. Gantt B, Meskhidze N, Kamykowski D. 2009 A new physically-based quantification of marine isoprene and primary organic aerosol emissions. *Atmos. Chem. Phys.* **9**, 4915–4927. (doi:10.5194/acp-9-4915-2009)
107. Weber J, Archer-Nicholls S, Abraham NL, Shin YM, Griffiths P, Grosvenor DP, Scott CE, Archibald AT. 2022 Chemistry-driven changes strongly influence climate forcing from vegetation emissions. *Nat. Commun.* **13**, 7202. (doi:10.1038/s41467-022-34944 -9)
108. Schmale J, Arnold SR, Law KS, Thorp T, Anenberg S, Simpson WR, Mao J, Pratt KA. 2018 Local arctic air pollution: a neglected but serious problem. *Earth's Future* **6**, 1385–1412. (doi:10.1029/2018EF000952)

Downloaded from royalsocietypublishing.org/rsta/article-pdf/doi/10.1098/rsta.2025.0269/6174177/rsta.2025.0269.pdf
by German Aerospace Centre (DLR) user
on 27 October 2026

109. Oltmans SJ *et al*. 2006 Long-term changes in tropospheric ozone. *Atmos. Environ.* **40**, 3156–3173. (doi:10.1016/j.atmosenv.2006.01.029)
110. Peterson PK, Pratt KA, Shepson PB, Simpson WR. 2025 Impacts of arctic oil field NO*x* emissions on downwind bromine chemistry: insights from 5 years of MAX-DOAS observations. *Faraday Discuss.* **258**, 293–306. (doi:10.1039/D4FD00164H)
111. Bauguitte SJB *et al*. 2012 Summertime NO_x measurements during the CHABLIS campaign: can source and sink estimates unravel observed diurnal cycles? *Atmos. Chem. Phys.* **12**, 989–1002. (doi:10.5194/acp-12-989-2012)
112. Zhai S *et al*. 2024 Transpacific transport of asian peroxyacetyl nitrate (PAN) observed from satellite: implications for ozone. *Environ. Sci. Technol.* **58**, 9760–9769. (doi:10.1021/acs.est.4c01980)
113. Luhar AK, Woodhouse MT, Galbally IE. 2018 A revised global ozone dry deposition estimate based on a new two-layer parameterisation for air-sea exchange and the multi-year MACC composition reanalysis. *Atmos. Chem. Phys.* **18**, 4329–4348. (doi:10.5194/acp-18-4329-2018)
114. Pound RJ, Sherwen T, Helmig D, Carpenter LJ, Evans MJ. 2020 Influences of oceanic ozone deposition on tropospheric photochemistry. *Atmos. Chem. Phys.* **20**, 4227–4239. (doi:10.5194/acp-20-4227-2020)
115. Saiz-Lopez A, Fernandez RP, Ordóñez C, Kinnison DE, Martín JCG, Lamarque JF, Tilmes S. 2014 Iodine chemistry in the troposphere and its effect on ozone. *Atmos. Chem. Phys.* **14**, 13 119–13 143. (doi:10.5194/acp-14-13119-2014)
116. Carpenter LJ, MacDonald SM, Shaw MD, Kumar R, Saunders RW, Parthipan R, Wilson J, Plane JMC. 2013 Atmospheric iodine levels influenced by sea surface emissions of inorganic iodine. *Nat. Geosci.* **6**, 108–111. (doi:10.1038/ngeo1687)
117. Tinel L, Adams TJ, Hollis LDJ, Bridger AJM, Chance RJ, Ward MW, Ball SM, Carpenter LJ. 2020 Influence of the sea surface microlayer on oceanic iodine emissions. *Environ. Sci. Technol.* **54**, 13 228–13 237. (doi:10.1021/acs.est.0c02736)
118. Yang M *et al*. 2025 Marine biogeochemical control on ozone deposition over the ocean. *Geophys. Res. Lett.* **52**, e2024GL113187. (doi:10.1029/2024GL113187)
119. Kilgour DB, Novak GA, Claflin MS, Lerner BM, Bertram TH. 2024 Production of oxygenated volatile organic compounds from the ozonolysis of coastal seawater. *Atmos. Chem. Phys.* **24**, 3729–3742. (doi:10.5194/acp-24-3729-2024)
120. Prados-Roman C, Cuevas CA, Fernandez RP, Kinnison DE, Lamarque JF, Saiz-Lopez A. 2015 A negative feedback between anthropogenic ozone pollution and enhanced ocean emissions of iodine. *Atmos. Chem. Phys.* **15**, 2215–2224. (doi:10.5194/acp-15-2215-2015)
121. Cuevas CA *et al*. 2018 Rapid increase in atmospheric iodine levels in the North Atlantic since the mid-twentieth century. *Nat. Commun.* **9**, 1452. (doi:10.1038/s41467-018-03756 -1)
122. Legrand M, McConnell JR, Preunkert S, Arienzo M, Chellman N, Gleason K, Sherwen T, Evans MJ, Carpenter LJ. 2018 Alpine ice evidence of a three-fold increase in atmospheric iodine deposition since 1950 in Europe due to increasing oceanic emissions. *Proc. Natl Acad. Sci. USA* **115**, 12 136–12 141. (doi:10.1073/pnas.1809867115)
123. Zhao X, Hou X, Zhou W. 2019 Atmospheric iodine (^{127}I and ^{129}I) record in spruce tree rings in the northeast Qinghai-Tibet Plateau. *Environ. Sci. Technol.* **53**, 8706–8714. (doi:10.1021/acs.est.9b01160)
124. Liao Z, Zhang J, Gao M, Ma Z. 2025 Widespread stratospheric intrusion influence on summer ozone pollution over China revealed by multi-site ozonesonde and validated EAC4 reanalysis. *Atmos. Chem. Phys.* **25**, 14 865–14 877. (doi:10.5194/acp-25-14865-2025)
125. Zhao K, Hu C, Yuan Z, Xu D, Zhang S, Luo H, Wang J, Jiang R. 2021 A modeling study of the impact of stratospheric intrusion on ozone enhancement in the lower troposphere over the Hong Kong regions, China. *Atmos. Res.* **247**, 105158. (doi:10.1016/j.atmosres.2 020.105158)
126. Dreessen J. 2019 A sea level stratospheric ozone intrusion event induced within a thunderstorm gust front. *Bull. Amer. Meteorol. Soc.* **100**, 1259–1275. (doi:10.1175/BAMS-D-18-0113.1)
127. Portafaix T, Morel B, Bencherif H, Baldy S, Godin-Beekmann S, Hauchecorne A. 2003 Fine-scale study of a thick stratospheric ozone lamina at the edge of the southern subtropical barrier. *J. Geophys. Res. Atmos.* **108**, 4196. (doi:10.1029/2002JD002741)
128. Nath D, Chen W, Graf HF, Lan X, Gong H, Nath R, Hu K, Wang L. 2016 Subtropical potential vorticity intrusion drives increasing tropospheric ozone over the tropical central pacific. *Sci. Rep.* **6**, 21370. (doi:10.1038/srep21370)

Downloaded from royalsocietypublishing.org/rsta/article-pdf/doi/10.1098/rsta.2025.0269/6174177/rsta.2025.0269.pdf
by German Aerospace Centre (DLR) user
on 27 October 2026

129. Nussbaumer CM, Fischer H, Lelieveld J, Pozzer A. 2023 What controls ozone sensitivity in the upper tropical troposphere? *Atmos. Chem. Phys.* **23**, 12 651–12 669. (doi:10.5194/acp-23-12651-2023)
130. Pouyaei A, Ginoux P, Naik V, Feng J, Horowitz LW, Paulot F. 2025 ENSO-Driven variability in ozone sources and its impact on tropospheric ozone radiative forcing. *Geophys. Res. Lett.* **52**, e2025GL115898. (doi:10.1029/2025GL115898)
131. Le T, Kim SH, Bae DH. 2022 Decreasing causal impacts of El Niño–Southern Oscillation on future fire activities. *Sci. Total Environ.* **826**, 154031. (doi:10.1016/j.scitotenv.2022.154031)
132. Le T, Kim SH, Heo JY, Bae DH. 2024 The influences of El Niño–Southern Oscillation on tropospheric ozone in CMIP6 models. *Atmos. Chem. Phys.* **24**, 6555–6566. (doi:10.5194/acp-24-6555-2024)
133. Yeh SW, Wang G, Cai W, Park RJ. 2022 Diversity of ENSO-related surface temperature response in future projection in CMIP6 climate models: climate change scenario versus ENSO intensity. *Geophys. Res. Lett.* **49**, e2021GL096135. (doi:10.1029/2021GL096135)
134. Liu Y, Cai W, Lin X, Li Z. 2022 Increased extreme swings of atlantic intertropical convergence zone in a warming climate. *Nat. Clim. Change* **12**, 828–833. (doi:10.1038/s41558-022-01445-y)
135. Zhou W, Leung LR, Lu J, Yang D, Song F. 2020 Contrasting recent and future ITCZ changes from distinct tropical warming patterns. *Geophys. Res. Lett.* **47**, e2020GL089846. (doi:10.1029/2020GL089846)
136. Taszarek M, Allen JT, Marchio M, Brooks HE. 2021 Global climatology and trends in convective environments from ERA5 and rawinsonde data. *npj Climate Atmos. Sci.* **4**, 35. (doi:10.1038/s41612-021-00190-x)
137. Sommariva R *et al.* 2026 Supplementary material from: Tropospheric Ozone Assessment Report II: Ozone distribution and variability in the oceanic and polar regions. Figshare. (doi:10.6084/m9.figshare.c.8638418)

Downloaded from royalsocietypublishing.org/rsta/article-pdf/doi/10.1098/rsta.2025.0269/6174177/rsta.2025.0269.pdf
by German Aerospace Centre (DLR) user
on 27 October 2026